Lisowiec, K., Słaby, E., Förster, H.-J. (2015): Polytopic Vector Analysis (PVA) modelling of whole-rock and apatite chemistry from the Karkonosze composite pluton (Poland, Czech Republic). - *Lithos*, *230*, p. 105-120.

DOI: http://doi.org/10.1016/j.lithos.2015.05.015

Polytopic Vector Analysis (PVA) modelling of whole-rock and apatite chemistry from the Karkonosze composite pluton (Poland, Czech Republic)

Katarzyna Lisowiec[a,b], Ewa Słaby[a], Hans-Jürgen Förster[c]

[a] Institute of Geological Sciences, Polish Academy of Sciences, Reasearch Centre Warsaw, Twarda 51/55, 00-818 Warsaw, Poland

[b] Institute of Geochemistry, Mineralogy and Petrology, University of Warsaw, Zwirki i Wigury 93, 02-089 Warsaw, Poland

[c] Helmholtz Centre Potsdam, GFZ German Research Centre for Geosciences, Telegrafenberg, 14473 Potsdam, Germany

Corresponding author:

Katarzyna Lisowiec

Institute of Geological Sciences, PASc

Twarda 51/55, 00-818 Warsaw, Poland

Phone number: +48 (22) 697 87 09

E-mail address: klisowiec@twarda.pan.pl

Abstract:

This study presents a novel approach for analysing the magma evolution path in composite plutons, applying the so-termed Polytopic Vector Analysis (PVA) to whole-rock and apatite chemistry. As an example of a multiphase magmatic body the Karkonosze granitoid pluton was chosen, which formed by a combination of magma mixing and fractional crystallization of two distinct melts – granitic crust-derived and lamprophyric mantle-derived. The goal was to model end-member magma compositions recorded by apatite and to estimate to what extent these end-members interacted with each other. Although using single minerals as proxies to magma compositions is tricky, the studied apatite well reflects the compositional trends within the magma (e.g. decreasing LREE/Y ratios, varying halogen content, increasing Mn and Na concentrations). The results of PVA simulations for whole-rock geochemistry demonstrate a model similar to that constrained from previous studies. Apart from the main trend of mixing between a felsic (~80 wt % SiO_2) and a mafic (~53 wt% SiO_2) end-member

(EM), an additional process has been recognized, representing most probably the continuous evolution of the mafic end-member, responsible for the compositional diversity of some rocks. One felsic (REE-poor, Mn−F-rich) and one mafic (Cl−Sr−Si−REE-rich) apatite end-member was recognized, whereas the third one represents most probably a fluid component (enriched in Si, Y, Ce and Nd), present at all magmatic stages, however, most prominent during the late stage. The widest range of EM proportions and the highest contribution of the mafic EM are displayed by apatites from the early stage. During the middle and late stages, the apatites present a narrow range of EM proportions, with almost all apatites bearing a felsic signature. This pattern reflects the progressive homogenization of the system. Although the PVA method applied to mineral chemistry poses some limitations, it may provide a more detailed image of the combination of differentiation processes and magma sources involved in the formation of a complex composite pluton.

Keywords: apatite, Polytopic Vector Analysis, magma mixing, Karkonosze, composite pluton

1. Introduction

Granitic rocks constitute a major part of the continental crust and provide insight into the processes of crust formation and recycling as well as mantle−crust interactions. They often form composite bodies, buildup of felsic ± intermediate ± mafic intrusions evolved by a combination of several differentiation processes, including fractional crystallization and magma mixing (e.g. Dokuz, 2011; Janoušek et al., 2004; Liu et al., 2013; Martins et al., 2013; Perugini and Poli, 2012; Perugini et al., 2003). One example of such a composite pluton is the well-studied granitoid massif of Karkonosze (SE Poland). Continuous evolution by fractional crystallization and occasional mixing of two compositionally distinct magmas (mantle- and crust-derived) gave rise to formation of various types of rocks of contrasting chemistry (Słaby and Martin, 2005, 2008). To define and quantify the differentiation processes involved in granite petrogenesis, geochemical modelling is required. One of the algorithms used to imitate the behavior of elements within magmatic systems are linear equations, employed both for fractional crystallization (in case of major elements) and magma mixing (major and trace elements, e.g. Fourcade and Allegre, 1981; Gourgaud and Villemant, 1992; Janousek et al., 2004; Rollinson,

1993; Słaby and Martin, 2008). However, linear equations can resolve only two end-member systems. Moreover, they assume that magmas from each stage of evolution (parental and evolved magmas, as well as magmas undergoing mixing) are collinear in terms of chemical composition. In case of Karkonosze batholith, K-feldspar studies demonstrated a non-linear element distribution between the subsequent magma batches (Słaby et al., 2011), resulting most probably from the presence of more than two end-members (mafic and felsic). This diversity is not perceptible in the whole-rock geochemistry which preserved the average information on the evolution processes. Therefore, supplementary studies of single mineral phases may provide a more detailed image of the results of the superimposed processes, enabling their recognition and distinction. A perfect candidate for a complementary investigation is apatite, as it usually hosts larger concentrations of trace elements compared to feldspar and, thus, is more sensitive to changes in the magmatic environment. Its usefulness in studying granite evolution, including magma mixing, has been confirmed by numerous authors (e.g. Broska et al., 2004; Chu et al., 2009; Dempster et al., 2003; Sha and Chappell, 1999; Szopa et al., 2013). Preliminary work on apatite from the Karkonosze pluton demonstrated that it is a suitable monitor of differentiation processes that occurred in the magmatic chamber (Przywóski, 2006; Słaby, 2006).

If multiple end-members (and/or sources) and evolution processes are involved, a multi-dimensional mathematical method may be useful to better characterize complex heterogeneous systems. Such task can be performed by Polytopic Vector Analysis (PVA). This is a multivariate statistical algorithm, which decomposes the chemistry of a system originated by mixing or unmixing (fractional crystallization) of two or more end-members and provides the estimate number and composition of these end-members and their proportions in every studied sample. The application of PVA to igneous systems enables evaluation of complex magmatic histories. Vogel et al. (2008) and Tefend et al. (2006) demonstrated the advantages of the method in distinguishing magma mixing from fractional crystallization, using modelled and natural rock compositions. The usefulness of PVA has also been confirmed by Szymański et al. (2013) who constrained a three end-member model for the formation of the Papagayo volcanic tuff deposits (Northern Costa Rica), which comprised several episodes of mixing/mingling. Constant influx of mafic magma into the magma chamber below the

Soufrière Hills lava dome (Montserrat) has been documented by Barclay et al. (2010), who used PVA to study the relationship between magmatic enclaves and their volcanic host rocks. A study done by Deering et al. (2008) demonstrated that PVA can be also applied to systems involving partial melting and crustal contamination. Up to now, the method was exclusively applied to whole-rock data, as they are the final result of all processes taking place in the magmatic chamber. We propose a novel application of PVA to single mineral compositions as proxies to magma geochemistry. A system, where magma mixing is one of the dominating processes, is composed of multiple magma domains interacting with each other mechanically and chemically (e.g. De Campos et al., 2008, 2011; Morgavi et al., 2013a; Perugini et al., 2003, 2008, 2012). A mineral crystallizing in such system may preserve signatures of those domains that will be lost in the final whole-rock chemistry. Therefore, as apatite is a useful petrogenetic indicator, it may represent the complexity of a magma mixing system in a much more detailed way than whole-rock geochemistry. End-members obtained based on apatite chemistry may serve to infer certain characteristics of the magmatic end-members participating during the mixing, e.g. enrichment in specific elements. However, using single minerals as proxies to magma compositions is tricky, as mineral chemistry is controlled by numerous factors, only one of which is magma chemistry. In consequence, such approach may present some risks, which we will attempt to evaluate.

The goal of this study is to apply PVA to apatite chemistry (as proxy to magma geochemistry) and whole-rock geochemical data of the Karkonosze pluton, in order to: 1) model end-member compositions recorded by apatite (compared to whole-rock) on every stage of magmatic evolution, 2) estimate to what extent these end-members interacted with each other and how many mixing/unmixing paths are present, and 3) verify the advantages and limitations of the combined PVA application in studying composite granitoid plutons. The choice of the well-recognized Karkonosze batholith as target allows a thorough comparison of the results (with previous studies) and verification of the new approach.

2. Geological setting

2.1. General information

The late- to post-collisional granitoid massif of Karkonosze (the Krkonoše–Jizera plutonic complex or the Krkonoše–Jizera pluton in the Czech literature and the Riesengebirge in German literature) is located at the north-eastern margin of the Bohemian Massif, which is a part of the Saxothuringian Zone of the Variscan orogen (Fig.1). It is one of the many magmatic bodies that intruded the orogenic belt during the late Carboniferous in a transpressional–transtensional tectonic setting (Mazur and Aleksandrowski, 2001). The shallowly intruded pluton formed by the multi-stage emplacement of several magma batches (Słaby and Martin, 2008; Žák et al. 2013).

The pluton has an E–W elongation of ~70 km and a minimal width of 20 km. Geochemically, it is predominantly composed of K-rich calc-alkaline granites (KCG) following the classification of Barbarin (1999). The Karkonosze granites bear variable signatures of A-type, I-type as well as S-type granites (Pin et al., 1987; Słaby et al., 2002, 2011; Wilamowski, 1998). According to recent age data, formation of the Karkonosze pluton extended over a time span of at least 20 Ma (Machowiak and Armstrong, 2007; Žák et al., 2013).

2.2. Petrography and evolution model

The Karkonosze pluton consists mainly of biotite-bearing porphyritic to equigranular granites and minor amounts granodiorites and quartz diorites. It is penetrated by numerous lamprophyric, felsic (aplitic, pegmatitic) and 'composite' dikes, which constitute mostly irregular, discontinuous bodies of various composition. The porphyritic granites (its primitive as well as evolved varieties) contain abundant microgranular magmatic enclaves (MME).

Petrology, mineralogy, geochemistry and tectonic setting of the Karkonosze batholith were extensively studied by numerous authors (Adamuszek et al., 2009; Awdankiewicz et al., 2005; Borkowska, 1966; Klominsky, 1969; Mierzejewski and Oberc, 1990; Patočka et al., 2000; Žak et al., 2006, 2013; Žak and Klominsky, 2007). Whole-rock and feldspar-chemistry investigations (Słaby and Götze, 2004; Słaby and Martin 2005, 2008; Słaby et al., 2002, 2007a,b, 2008, 2011) provided evidence that magma mixing and fractional crystallization were the dominant processes in batholith formation. An evolution model has been proposed (Słaby and Martin, 2008), according to which in the

course of continuous differentiation by fractional crystallization, two magmas of contrasting compositions – LREE-rich mantle-derived and LREE-poor crust-derived – interacted with each other periodically, giving rise to different types of rocks depending on the stage of pluton evolution. These rock types encompass granodiorites and porphyritic granites in the early stage, microgranular magmatic enclaves hosted by porphyritic granites in the intermediate stage and composite dikes in the late stage. Batches of equigranular granite and lamprophyric dikes represent rocks formed from 'pure' parental magmas that did not experienced mixing. In late stages, fluid overprint is especially manifested in composite dikes.

2.3. Samples

Nineteen samples were taken from various parts of the pluton, including lamprophyre (LAM1, LAM2), equigranular granite (HRA, EQU), primitive porphyritic granite (MIL), granodiorite (FOJ, RUD1, RUD2, VRE), evolved porphyritic granite (MICH, SPH), magmatic enclaves (ENK1 to ENK5, BUK) and composite dikes (SOK, GR). Their localization, degree of evolution and geographic coordinates are given in Table 1. Detailed petrographic description of all types of rocks assembling the Karkonosze pluton is provided by Słaby and Martin (2008).

3. Analytical methods

Rock samples (~3 kg) were crushed in a jaw crusher and sieved until ≥ 80% was in the 400 – 56 μm fraction. From this, accessory minerals (apatite, zircon, titanite, rutile, monazite, allanite) were separated using heavy liquids (sodium polytungstate). From these heavy-mineral separates, polished grain mounts were prepared. Since the textural context of minerals got lost in such separates, thin sections of all types of rocks were also analysed.

Grain mounts and thin sections were studied using scanning electron microscopy (SEM) and electron-microprobe analysis (EPMA). Basic textural investigation and back-scattered electron (BSE) images were conducted on a FEI Quanta 650 MLA-FEG (SEM) in the Geometallurgy Laboratory of the TU Bergakademie Freiberg, Germany, operated at 25 kV accelerating voltage and 1 nA beam current. The chemical composition of apatite (major + minor elements) was determined by wavelength-dispersive (WDS) X-ray analysis using a JEOL JXA-8500F (HYPERPROBE) field-emission electron microprobe at the Deutsches GeoForschungsZentrum (GFZ) in Potsdam, Germany,

applying the following analytical conditions: acceleration voltage of 20 kV, a beam current of 10 nA, and a beam diameter of 5 μm. The analytical conditions applied guaranteed minimal mobilization of Na and the volatiles both during standardization and spot analysis. Standards, measuring conditions and detection limits are given in Table 2. Background counting times were set to half of the representative peak counting time. Data processing was undertaken using the CITZAF routine, which is based on the Φ(ρZ) method (Armstrong, 1995). More than 1,000 single-spot analyses were performed in order to create a representative database for the PVA simulations.

4. Polytopic Vector Analysis (PVA)

Polytopic Vector Analysis is a method that is aimed at analysing a system formed by mixing of two or more components (end-members) and extracting the number, chemical composition and proportions of end-members (cf. Johnson et al., 2002; Vogel et al., 2008). The main principles of PVA are summarized below.

First, the compositional data is plotted into a geometric figure termed a polytope. Its vertices represent the calculated compositions of end-members that underwent mixing. Before running the simulations, the user has to estimate the number of end-members which is required to fully define the system. For that purpose, a coefficient of determination (so-termed Klovan/Miesch Coefficient of Determination – KMCD or simply CD) is calculated, which reflects the ratio between original values from the data set and values back-calculated by the algorithm for every number of end-members from a given range. The higher the CD, the more accurate is the assumption about the number of end-members. When the number of end-members is finally determined, the second step is to find the exact position and shape of the polytope within the generated multi-dimensional space, so that it encloses as many points from the data cloud as possible. This is achieved through subsequent iterations which modify the initial polytope until all data points are located within it and proportions of end-members in samples are positive.

PVA software used in this study was created and shared by Robert Ehrlich (Residuum Energy Inc., Salt Lake City, UT) and Thomas A. Vogel (Michigan State University, USA). Four basic simulations (runs) were performed, one for whole rock chemistry (with generated magmatic whole-

rock end-members) and three for apatite composition (with generated apatite end-members for early, middle and late stage). Table 3 presents the list of samples used in each run.

5. Results

5.1. Geochemistry of apatite

Compositional data and representative textures of apatites are listed in Table S8 (Supplementary Electronic Material) and shown in Fig. 2-6. The study of the distribution patterns of major and minor elements (the word minor refers to the method by which they were analysed, as electron microprobe is not designed for trace elements; however, for simplification the term 'trace' elements will be used in the following sections) in apatite from rocks representing all stages of magma evolution (mixing + fractional crystallization) and the relations between certain elements or groups of elements are crucial for defining the evolution path at micro-scale and necessary for a substantial evaluation of PVA results. Apatite growth textures are described for being one of the most important monitors of magma mixing.

Lamprophyres

Apatite grains form usually small (up to 50 µm in diameter), euhedral inclusions in mica or are scattered chaotically in the rock matrix. Apatite textures are similar in both samples (LAM1 and LAM2) and, in most cases, homogeneous in BSE image.

The composition of apatite from lamprophyres is distinct from that of apatite from the other rock types. It is characterized by variable, but generally elevated Sr and S contents (up to 1.9 wt% SrO in LAM2 and 0.55 wt% SO_3 in LAM1, resp.) accompanied by low (HREE+Y) abundances. The concentrations of light rare earth elements (LREE) are similar to those in apatite from the other rock types, but low compared to their host-rock abundances, which are highest among all rocks assembling the pluton. The LREE/Y ratio is most elevated (Fig.4). The apatite is further characterized by moderately high Na and Cl contents (higher in LAM1, Figs.5 and 6) and low Mn concentrations (~ 200–1200 ppm, Fig.5).

Granodiorites

Apatite grains usually occur as 50–250-µm-sized inclusions in mica and feldspar or are interstitial between major phases. They are distinguished by the most complex zonation patterns,

including irregular, discontinuous to oscillatory zoning, resorption boundaries and syneusis textures (Figs.2a-c). Single grains may contain multiple zones displaying varying BSE-intensity.

Apatite composition spans a wide range, depending on the type of granodiorite and domain within the grain. Lanthanides show the largest variations in concentration and are the components most significantly triggering BSE-intensity. Their total concentrations may vary up to several thousand ppm within a single grain (e.g. grain apa2) and approach 3.5 wt% in granodiorite RUD1 and 1.5 wt% in granodiorite FOJ. Generally, the apatites are characterized by LREE-enrichment, similarly to apatite I-type and S-type granites (Broska et al., 2004) and mafic I-type granites (Sha and Chappell, 1999). Apatite from the FOJ sample shows a bimodal distribution on the LREE vs. Y and Mn vs. Na plots. One population (apatite in grain mounts or hosted in feldspar) is characterized by a high LREE/Y ratio (Fig.4a) and low contents of Mn and Na (Fig.5a), whereas the other (apatite included in biotite) displays a low LREE/Y ratio, together with comparatively larger Mn and Na concentrations (Figs. 4a and 5a). Apatite from samples RUD1 and RUD2 plots between the two trends of the FOJ sample on the LREE vs. Y plot, with some spots overlapping the EQU and HRA trend (Fig.4b). They exhibit low Mn contents and a wide range of Na concentrations (Fig.5b). Apatite from the VRE sample matches the LREE /Y ratio of EQU and HRA apatite (Fig.4b) and has substituted Mn- and Na-contents in concentrations similar to apatite from RUD1 and RUD2 granodiorites. Generally Mn and Fe contents in apatite from all granodiorites are consistent with I-type granites of Broska et al. (2004) and Sha and Chappell (1999), however, some values fall in the A-type and S-type field.

Within the group of granodiorites, the FOJ type apatite has incorporated the largest concentrations of Cl (up to 800 ppm; Figs. 6a-b) which are, however, lower than those recognized in apatite from the lamprophyres. Chlorine concentrations of that order of magnitude correspond to those of apatite crystallized in I-type and A-type granites (Broska et al., 2004; Sha and Chappell, 1999). Apatite from the RUD1, RUD2 and VRE samples contains still lower Cl and higher F (Fig.6b), which are consistent with S- and A-type origin of these granites (Broska et al., 2004).

Porphyritic granites

Apatite mostly occurs as 100−200-μm-sized euhedral to subhedral inclusions in mica or feldspar or interstitially. Growth textures range from complex – irregular and discontinuous zoning

with numerous resorption boundaries (samples MIL and MICH, Fig. 2d and Fig. 3a) to more simple – homogenous or oscillatory zoning (sample SPH, Fig.3b).

Apatite composition in the various porphyritic varieties of the batholith shows evolution of elemental contents and ratios reflecting the progress of differentiation, allowing to easily distinct apatite from the "primitive" samples (MIL, MICH) from that precipitated in the evolved one (SPH). Apatite from the least evolved porphyritic granite (MIL) compositionally resembles that from the granodiorites, with some minor differences. It exhibits a slightly higher (compared to FOJ apatites) Cl content (up to 2,000 ppm, Fig.6b), combined with a wide range in F concentration (3.3–3.8 wt%) and a slightly elevated Sr content (reaching 400 ppm). Total REE-content is similar to that of apatite from the FOJ granodiorite, but the Y-content is relatively lower. Similarly to FOJ apatites, there is a slight bimodality on the LREE/Y diagram, with the majority of grains showing high LREE/Y ratios (Fig.4c). Apatite from the MICH sample displays similarly high LREE/Y ratios, but no bimodality (Fig.4c), but its Cl content, reaching ~300 ppm, is substantially lower than that in MIL apatite (Fig.6c). Concentrations of Mn and Na are similar in apatite from both "primitive" samples (Na content lower than in apatite from lamprophyres, Mn content lower than in apatite from the equigranular granite, see Fig.5e). Mn and Fe concentrations in MIL apatite straddle the fields of I-, S and A-type granites as defined by Broska et al. (2004). MICH apatites, however, show Mn and Fe contents typical of S-type granites (Broska et al., 2004; Sha and Chappell, 1999). Apatite from the evolved granodiorite is characterized by (a) a significantly lower Cl content (Fig.6c), (b) Sr concentrations below detection limit, (c) relatively larger HREE abundances and (d) Mn and Na contents similar to those in apatite from the equigranular granite and lamprophyre, respectively (Fig.5e). The LREE/Y ratio in apatite from this rock is similar to that of apatite from the EQU granite and lower than in apatite from the granodiorites and primitive porphyritic granites (Fig.4c). Low Cl, higher Mn and a slight HREE-enrichment are broadly consistent with the respective patterns of apatite originating from S-type granites (Broska et al., 2004; Sha and Chappell, 1999).

Microgranular magmatic enclaves

Enclaves contain small apatite inclusions (up to 100 μm in diameter) hosted in mica and feldspar. Growth textures are less complex and dominated by oscillatory zoning (Fig.3c,d). There are only subtle differences in BSE-intensity between adjacent zones. Patchy zonation is subordinate.

Chemical composition of apatite from samples ENK1 to ENK5 is relatively uniform, but distinct from that of apatite from the BUK enclave. Single-grain variations in concentration are small in apatite from the ENK samples for most trace elements, except for Y and Si, which show strong fluctuations of up to 1 and 0.6 wt%, respectively, between adjacent domains. The BUK apatite exhibits just opposite patterns, with significant compositional variations in single grains of all trace elements, especially REEs and Y. Moreover, whereas ENK apatite contains up to 600 ppm Cl (similar to apatite from I-type granites; Broska et al., 2004), the BUK apatite contains Cl in concentrations usually below the detection limit as typical for S-type magmatites (Fig.6d). Na and Mn contents are slightly different for every enclave and plot either between apatite from the lamprophyres and equigranular granites or below apatite from lamprophyres on the Mn vs. Na diagram (Fig.5d).The main distinction between apatite from the ENK and BUK enclaves consists in the REE composition. Whereas the BUK apatite shows a high LREE/Y ratio (even slightly higher than in apatite from granodiorites), in ENK apatite, this ratio is identical to that of SPH and EQU apatites (Fig.4d). Both types of enclaves demonstrate LREE-enrichment typical for apatite from I-type granites (Broska et al., 2004).

Composite dikes

Apatite forms 50–250-μm-sized, euhedral to subhedral grains usually hosted in or attached to mica and feldspar. The GR sample contains mostly homogeneous and two-zoned (core and rim) apatite grains, whereas apatite from the SOK sample usually demonstrates complex irregular zoning (Fig.3e).

Apatite from the studied dikes is compositionally similar, but not identical. Chlorine content is quasi-identical and reaches ~300 ppm. The concentration of Sr is significantly higher (up to 600 ppm) in SOK apatite, usually in BSE-darker domains. Na and Mn concentrations are consistently low (Fig.5c). The main distinction between the two samples is the LREE/Y ratio. The SOK apatite exhibits a high LREE /Y ratio that partly overlaps that of apatite from the EQU granite (Fig.4e). Apatite from the GR dike is higher in Y, resulting in lower LREE/Y ratios that are similar to those of apatite from the EQU

granite (Fig.4e). The composition of apatites from both composite dikes is consistent with apatites forming from I-typegranite magmas (Broska et al., 2004; Sha and Chappell, 1999).

Equigranular granite

Apatite forms usually small (up to 80 μm in diameter), euhedral to subhedral grains hosted in or attached to mica. It displays simple growth textures, from homogeneous to oscillatory zoned (Fig.3f). Grains consist typically of a BSE-dark core and a BSE-bright rim. The oscillatory zoning is very subtle, with no sharp boundaries between domains.

Chemical composition of apatite is distinct from that of the lamprophyres. The apatite is generally Y-rich, thus possessing a lower LREE/Y ratio (Fig.4. Total REE abundance of EQU apatite is similar to, while that in HRA apatite is higher than that recognized in the apatite from lamprophyres (Table 4). The contents of Sr, S and Cl are mostly below detection limit (Fig.6). In contrast, the concentrations of Mn and Na are high (higher in HRA apatite, cf. Fig.5). High Y and Mn concentrations, together with low Cl, correspond with the compositional signatures of apatite crystallizing in S-type granites of Broska et al. (2004) and felsic I-type and S-type granites of Sha and Chappell (1999).

5.2. PVA modelling

Whole-rock composition

PVA of whole-rock composition (run Whole-rock All) included 51 samples (representing all rock types from the Karkonosze batholith) previously analysed by Słaby and Martin (2008) (Table 3).Chemical composition of the generated end-members is given in Table 4. Selection of three end-members was optimal, as KMCD's for all elements are sufficiently high (usually >0.6 for trace elements and >0.7 for major elements, Table 5). The addition of the fourth end-member improved the KMCD's, but the generated end-members displayed unrealistic compositions (one EM with SiO_2 ~ 38 wt% and one EM with SiO_2 ~81 wt%). Based on the major-element composition, one felsic (EM1) and two mafic (EM2 and EM3) end-members were discriminated. EM2 and EM3 model compositions are similar to those of the lamprophyres, at least in terms of major elements. Modelled EM1 is devoid of Ti, Fe, Mn, Mg, Ca and P. It is generally depleted in trace elements compared to the mafic end-members, except for Rb and Th. EM2 is the mafic end-member that is generally rich in trace elements,

such as Ba, Th, Sr, Zr, Ni and REEs, however, EM3 is modelled having higher concentrations of Na, Y, Rb and Nb relative to EM2.

Fig. 7 demonstrates the proportions of whole-rock end-member in all samples. The line along the EM2 – EM1 side of the triangle is consistent with mixing (and/or fractional crystallization) between felsic and mafic end-members and implies the following sequence of rock types (with decreasing contribution of EM2): lamprophyres → granodiorites → composite dikes → porphyritic granites → equigranular granites. Lamprophyres concur with the mafic end-members (either EM2 contaminated slightly by EM1 or a mixture of EM2 and EM3). The trends formed by granodiorites and enclaves, which extend from the EM2 – EM1 mixing line towards EM3, indicate that the second mafic end-member mixed with magmas evolving along the main trend of evolution, intersecting the EM2 – EM1 line at ~55% EM2, 40% EM1 and 5% EM3 for granodiorites and 65% EM1, 25% EM2 and 10% EM3 for magmatic enclaves. The contribution of EM3 can approach ~90% in granodiorites and 40–60% in mafic enclaves. In most composite dikes and porphyritic granites, EM2 is the dominating mafic end-member, except for one composite dike (COM-1 from Słaby and Martin, 2008, with composition similar to GR) and one porphyritic granite (POR-11 from Słaby and Martin, 2008, moderately evolved) with 35% and 26% of EM3, respectively. The equigranular granites contain the largest proportions of EM1. Most of the EQU samples contain minor contributions of both the mafic end-members EM2 and EM3, however, three EQU samples are located on the border of the diagram with EM2=0%

Apatite composition

PVA of apatite composition was performed in three runs (Apatite Early Stage, Apatite Middle Stage and Apatite Late Stage), in order to recognize the apatite end-members stage by stage. The selection of samples for each stage is given in Table 3. To simplify the simulations, apatite from the first intruded , primitive rocks is considered early (similarly as in middle and late stages), even though the samples may contain multi-stage populations of apatite. Further subdivision of apatite in single samples would have excessively complicated both the input and output data. Additionally to apatite from the respective host rock, each run considered apatite from lamprophyre and equigranular granite as potential end-members in magma mixing (Słaby and Martin, 2008).

Chemical composition of the end-members generated from every run is provided in Table 6. In each simulation, a 3-end-member solution characterized the data sufficiently well. KMCD's for all oxides are usually >0.5 for the majority of elements (Table 7). The elements displaying the lowest KMCD's include Th, U, Yb, Mn, Fe, Na and Sr. The poor fit for Th, U, Yb and Sris likely related to their generally low contents at or below the limit of detection. The variations in concentrations of Fe and Na could be ascribed the variable presence of additional Fe and Na sequestering species (preferentially biotite and plagioclase) in the individual rocks. With four end-members, the KMCD's would improve weakly (more significantly in case of U), however, the fourth end-member would have an almost identical composition as the felsic apatite end-member.

Apatite end-members obtained from the simulations are compositionally distinct, however, the differences are not serious. The PVA algorithm processes the input data in the way that it searches for most extreme compositions (in terms of single elements or groups of elements) and considers them potential end-members, which are being modified in the subsequent iterations. The elements showing the largest variations have also the highest KMCD's and may display major differences between the generated end-members. In the situation of only few of such elements, the composition of end-members is generally similar.

EM1 is a pure fluoroapatite devoid of all trace elements (S, Sr, Cl, Y, REEs) in the early stage, while in the middle and late stages, the modelled concentrations of these elements are significantly higher. EM2 has non-stoichiometric P- and Ca concentrations, which are compensated by elevated Si, Y and REE (reflecting the substitution reaction $P^{5+} + Ca^{2+} \leftrightarrow Si^{4+} + (REE,Y)^{3+}$). It is most enriched in these elements in the middle stage. EM3 is a water- and Cl-rich apatite, with high Sr- and S contents and average REE concentrations. The concentrations of LREEs, Sr, S and Cl systematically decrease from the early to the late stage, whereas Mn and Si display the opposite trend.

Proportions of the apatite end-members for every stage are demonstrated in Fig. 8−10. Distribution of points on the ternary plot for the 3AE run shows a nicely ordered sequence of rock types (Fig.8). Apatite from lamprophyres has incorporated the largest contribution of EM3. Apatite from "homogenized" granodiorite (FOJ) has a wide range of proportions, with a contribution of EM3 being second largest after apatite from lamprophyres. A slightly lower contribution of EM3 is manifested in

apatite from the primitive porphyritic granite, followed by apatite from the less homogenized granodiorites (RUD1, RUD2, VRE). The highest contribution of EM1 refers to apatite from the equigranular granite.

In the 3AM run, the contribution of EM3 is again largest (up to 70%) in lamprophyric apatite, but apatite from the samples representing the middle stage are all positioned very close to EM1 vertex, implying <10% of EM3 (Fig.9). The individual populations usually overlap. No differences are demonstrated between the proportions of EM1 and EM3 in apatite from enclaves and their host porphyritic granite. Apatite from equigranular granite again displays the largest contribution of EM1.

The late stage simulated by the 3AL run yielded similar results in terms of end-member proportions (Fig.10), with the exception of higher content of EM2. Apatite from all composite dikes and the equigranular granite is located within the EM1 – EM2 line, containing <10% of EM3. In the late stage, apatite from lamprophyres contains the greatest proportion of EM3.

6. Discussion

6.1. PVA-based whole-rock evolution model

PVA modelling of the whole-rock presents the evolution path of the Karkonosze magmatic system in a way slightly different from previous studies. The general sequence of samples along the EM2 – EM1 mixing line in the ternary diagram (Fig.7) is consistent with the existing evolution model (cf. Słaby and Martin, 2008). The felsic end-member (EM1) has a strongly evolved composition, as it contains minor amounts of compatible elements. Certainly, it does not represent the felsic parental, but highlights the theoretically most evolved granitic magma at the final end of fractional crystallization. Indeed, most equigranular-granite samples are located closest to the EM1 vertex. The equigranular sample with the least contribution of the EM1 is HRA, which most likely identifies the primitive granitic parental magma.

Apart from the decreasing EM2/EM1 ratio, the second feature that differentiates the rock types is the varying proportions of EM2 and EM3. Whereas porphyritic granites and most of lamprophyres and composite dikes contain very little EM3 (implying that the mafic melts involved in their formation were compositionally very similar), granodiorites and enclaves have varying proportions of both mafic end-members. We interpret EM2 and EM3 not as separate and independent mafic end-members, as the

whole-rock composition did not point to two unlinked mafic sources. Most likely, they represent a more primitive (EM2) and a more evolved mafic magma (EM3). Subsequent mafic-magma inflows differed in terms of chemistry (due to the differentiation of the mafic melt), giving rise to varying granodiorite and enclave compositions indicated by the spread of these rocks between EM2 and EM3. Previous studies assigned this diversity among granodiorites (and, separately, among the enclaves) merely to varying proportions of the felsic vs. mafic magma, with the suggestion that the mafic melt evolved between the early and middle stages. Present results, however, indicate that the compositional variations were additionally caused by the evolution of the mafic end-member during individual stages (not only between them). The evolution of the mafic melt by fractional crystallization was already previously supposed, but not evidenced (Słaby and Martin, 2008; Słaby et al., 2011). PVA results strongly support this mode of magma evolution.

PVA results gave evidence of the existence of multiple end-members and their interaction is responsible for the compositional diversity among the studied rocks. Based on previous studies, individual processes could have been recognized in the ternary diagrams – major mixing between lamprophyres and equigranular granite (accompanied to some degree by fractional crystallization of the felsic end-member), evolution (probably by FC) between EM3 and EM2 marked by granodiorites and enclaves and, finally, major mixing combined with evolution of the mafic end-member. It is obvious that almost all samples – and especially enclaves and granodiorites − formed from a complex mixture of more than two components and that a two end-member system (supposed from previous studies) is not sufficient to account for such a wide range of compositions.

6.2. Apatite as proxy for magma compositions

Apatite is considered constituting a petrogenetic tracer (e.g., Belousova et al., 2002; Broska et al., 2004; Buda and Pal-Molnar, 2012; Chu et al., 2009; Sha and Chappell, 1999; Spicer et al., 2006) that reflects the composition of the host magma and monitors differences in chemistry between different rock types. The results of this study corroborate this assessment. Apatite composition follows the chemical evolution of the Karkonosze magmas and shows features characteristic for both I-type (mafic and felsic) and S-type granites. However, in order to use apatite chemistry as a proxy for end-member

magma compositions in PVA geochemical modelling, its capability of accurately tracing the real changes in magmatic environment has to be evaluated.

The composition of a mineral crystallizing from a magma is controlled by numerous factors, of which the most important are melt composition, temperature, mineral/liquid partition coefficients, oxygen fugacity, diffusion rates, local saturation conditions and presence of competing phases. If crystallization takes place at equilibrium conditions (and trace elements are incorporated according to the Henry's Law), at least on a local scale, the composition of a mineral will directly reflect the composition of the liquid from which it crystallized. The studied apatite, however, normally displays disequilibrium textures, including sharp zoning and resorption boundaries, especially in the early, primitive samples (FOJ, MIL, RUD1, RUD2, MICH) and, subordinately, in magmatic enclaves and composite dikes. Such textures are usually interpreted as reflecting a heterogeneous magmatic system, dominated by magma mixing (e.g. Streck, 2008; Tepper and Kuehner, 1999; Ginibre and Wörner, 2007). Each discrete growth zone may represent a magma domain of different composition. Although such interpretation is consistent with previous studies (Słaby and Martin, 2008; Słaby, 2006; Przywóski, 2006), other possible reasons for compositional variability need to be addressed.

One of the processes generating zoning in minerals is the kinetically-driven element extraction from the melt, involving the creation of a boundary layer in the closest vicinity of the crystal (due to delayed diffusion of elements within the melt), depleted in compatible elements (e.g. REE, Y) and enriched in incompatible elements. Since the list of elements measured in this study does not contain any incompatible elements in apatite, the relations between compatible and incompatible elements cannot be verified. However, in case of most complex textures and largest compositional variations within single grains from this study, the differences in elemental concentrations (> 6,000 ppm in case of both REE and Y) are too large as to attribute them to the boundary-layer effect (cf. Dempster et al., 2003). Therefore we conclude that greater element variations causing distinct zonation are not the result of delayed diffusion of elements between the surrounding layer and bulk magma, but rather indicate crystallization from compositionally different magma domains.

Another reason for the formation of zonation textures is supersaturation due to undercooling (e.g., temperature difference on the contact of hotter, mafic melt with colder, granitic magma). A system

dominated by magma mixing contains various magma domains, each with different (more felsic or mafic) composition and, consequently, temperature. Mineral crystallizing on the interface between hot and cold magma may, therefore, be subjected to undercooling, causing increased (non-Henrian) uptake of compatible elements (Morgan and London, 2003), however, owing the lacking information on incompatible elements, this hypothesis could not be tested. The comparison of compatible vs. incompatible elements in feldspar, however, points to domination of near-equilibrium conditions during its crystallization (Słaby et al., 2008). Both feldspar and apatite are early-crystallizing phases, therefore, it is feasible to assume that similar conditions were present also during the formation of apatite.

A further factor that has a large impact on apatite's ability to record magma composition is the diffusion rate of elements during the chemical exchange between the mixing magma domains. Trace elements diffuse with different rate (diffusive fractionation), therefore, the partially mixed magma domains may not show linear trace-element relations as suspected during magma mixing (Perugini et al., 2006, 2008, 2013). For instance, since Na has higher diffusion rates than LREEs (Morgavi et al., 2013a, 2013b; Perugini et al., 2008, 2012, 2013), mixing magma domains will exchange Na faster than Ce. Apatite grains growing in such domains will miss zoning in Na content and, thus, will monitor the average Na concentration of the melt (the initial Na content of the mingling parental magmas before homogenization will not be preserved). In contrast, LREE concentrations will be either higher or lower, depending on the domain from which the apatite crystallized. The transfer of apatite between LREE-poor and LREE-rich domains will produce distinct zonation patterns as observed in most of the studied apatite grains. As a result of different diffusion rates, elemental relations in apatite will normally not fully represent those of parental magmas. It has to be noted that diffusive fractionation (similarly as temperature difference) will influence apatite composition mostly in the early to middle stages of magmatic evolution, when magma mixing was the dominating or, at least, significant process. In the rocks which formed mostly due to fractional crystallization (e.g. SPH, HRA, EQU), apatite probably reflects the magma composition to a greater extent.

Although some extreme apatite compositions may be the result of "chaotic" incorporation of trace elements typical for a mixing-dominated regime, we assume that variations in trace-element content

generally reflect the heterogeneity of the magma and, thus, the complexity of the Karkonosze magmatic system better than does the whole-rock chemistry. Therefore, application of apatite chemistry in PVA provides additional important information.

6.3. Evidence of processes in the early stage of magma evolution recorded by apatite

Chemical composition of apatite from the early emplaced rocks (granodiorites, primitive porphyritic granite) reflects the general characteristics of their host magmas. Previous whole-rock and feldspar studies show that the mafic end-member derived from the metasomatized mantle was enriched in, for instance, LREE and Sr (Słaby and Martin, 2005, 2008; Słaby et al., 2007a, b), a signature also displayed by apatite. Characteristics typical of both I-type and S-type granites suggest that both mafic and felsic melts contributed to the formation of apatites.

Apatite end-members of the early stage generated by PVA are partially compatible with the measured apatite composition. The greatest similarity is observed for the mafic end-member. EM3 apatite is enriched in REEs, Cl, Sr, Na and S and depleted in Mn and Y compared to the felsic apatite (EM1), as is apatite from lamprophyres and granodiorites. Dividing the REE content of the mafic apatite by the REE content of the most primitive lamprophyre (Słaby and Martin, 2008), as well as PVA-generated whole-rock mafic end-member, provides partition coefficients similar to those reported in literature (Nagasawa, 1970; Fujimaki, 1986). In the latter case, the calculations support the validity of the PVA-generated mafic end-member. Elevated Cl content in mafic apatite is in line with the results of Patiño Douce et al. (2011), who described Cl- and H_2O-rich apatite from metasomatized enriched mantle. Although apatite composition is controlled by many factors, such elevated Cl content reflects the specific composition of the metasomatizing fluid, which is Cl- and H_2O-rich. Studies of the volatile inventory in apatite revealed a general trend of decreasing Cl content and increasing F/Cl ratio from more mafic to more felsic rocks (Marks et al., 2012). Indeed, primitive granite varieties, that experienced the highest degree of mixing, such as MIL granite and FOJ granodiorite, contain Cl-rich apatite, providing an additional argument for the supposed contribution of large amounts of mafic magma derived from metasomatized mantle regions. Apatite from these samples is also located closest to the mafic end-member on the PVA tertiary diagram (Fig.8). High S content and low Mn

concentrations (both in apatite and modelled mafic apatite end-member) are also characteristic for apatite from mafic I-type granites (Sha and Chappell, 1999).

Certain apatites from the EQU granite and even from some granodiorites are trace element-poor and are located very close to the EM1 vertex, however, never exactly on it. However, the composition of the felsic apatite end-member (EM1) being devoid of all trace elements is geologically unrealistic. Puzzling is also its unexpectedly high Fe content (which should not be the case as the mafic melt is more Fe-rich) and excessive F. Even though apatite data served as an input for PVA simulations, one cannot expect the programme to generate real, stoichiometric apatite compositions. Apatite chemistry serves as a proxy to magma compositions, therefore the end-members are only approximations and simply reflect certain enrichments or depletions of elements which can then be transferred to whole-rock chemistry. The absence of REEs and high F is most probably caused by the method itself and cannot be influenced by the user. The high Fe content EM1 however, is likely attributed to the high Fe concentrations in apatite from the equigranular granite (and partially also granodiorites). These, in turn, are most probably analytical artefacts, caused by the excitation of Fe from the adjacent Fe-rich biotite. Therefore, the Fe content implied for EM1 is unrealistic as well. The paucity in trace elements in EM1 is compensated by the presence of EM2, which is trace element-rich. The exceptional enrichment of EM2 in REEs, Y and Si and its high proportions in many apatite zones, may reflect two features. The first is the participation of a third component, possibly representing a fluid phase, exsolved from the coexisting magmas. The activity of fluids was documented in the late stages of the pluton formation (Słaby, 2006) and was associated mainly with late composite dykes. The apatite composition and PVA-generated end-members, however, indicate that the fluids might have been present already during the early stages of pluton formation. The second hypothesis which could explain the unusual composition of EM2, and which has been mentioned in section 6.2., is the chaotic incorporation of elements in apatite (possibly due to supersaturation). If certain apatite zones are enriched in trace elements due to supersaturation, the existence of trace element rich end-member is necessary to account for such high concentrations. Consequently, the composition of EM2 may not necessarily reflect the existence of a separate trace element-rich component. However, as supersaturated conditions occurred only locally, they cannot be responsible for high trace element

contents in a large number of apatites. Therefore, the participation of a Y- and REE-rich fluid phase is more plausible.

The proportion diagram (Fig.8) shows a nicely ordered sequence of decreasing contribution of the mafic apatite end-member from lamprophyre, primitive porphyritic granite, granodiorite (in the order FOJ – RUD1, RUD2, VRE) to equigranular granite. This sequence is in general agreement with the evolution model, however, there is a discrepancy regarding the LAM1 and LAM2 samples. The PVA-generated mafic apatite does not fully correspond to LAM1 and LAM2 apatite since these are displaced from the EM3 vertex (Fig.8). Although LAM2 is a more primitive lamprophyre (and the lamprophyric magma was primitive in this stage of evolution), it is located more distant from the EM3 vertex. Most probably, the composition of the apatite from LAM2 is not sufficiently distinct from that of apatite from the granodiorites, so the algorithm chose the more extreme composition of apatite from LAM1 as the closest approximation of the potential mafic apatite. The location of apatite from the primitive lamprophyre (LAM2) on the proportion diagram may be also due to the heterogeneity of the mantle source. Late lamprophyric dikes might have been extracted directly from the mantle. Despite the fact that LAM2 is primitive in composition, it does not have to fully correspond to the primitive lamprophyric melt participating in mixing with the granitic magma, as it might have been extracted from a slightly different mantle region. Their composition is often a result of combined partial melting of the heterogeneous mantle, source mixing, shallow-level differentiation processes and crustal contamination (Awdankiewicz, 2007).

Apatites from the FOJ granodiorite and MIL granite are compositionally similar and plot nearby on the PVA proportion diagram. FOJ apatites have the widest range of proportions of both felsic and mafic end-members (Fig.8). Such spread is consistent with what was observed for feldspars, implying that during the formation of this type of granodiorite, the compositional gradient between coexisting magmas was greatest, which indicates that during the early crystallization stages, the mafic and felsic melts were not yet homogenized (Słaby et al., 2007a,b). A similar, but slightly narrower range of EM1/EM2 proportions is represented by MIL apatite. A significant contribution of the mafic end-member in MIL apatite is in contrast to what was established from the whole-rock chemistry which suggested significantly lower proportions of mafic magma contributing to the formation of this granite

(Słaby and Martin, 2008). The diversity of apatites from both FOJ and MIL samples (and relatively large proportions of the mafic end-member) is also reflected in varying LREE/Y ratios and Na-, Mn and F contents. Two populations separated by their LREE/Y and Na/Mn ratios (in case of MIL apatite only LREE/Y ratios) point to at least two stages of apatite formation. The population with the higher LREE/ Y and Na/Mn ratios consists only of apatites from the mineral separates, which probably represent early crystallized single crystals and not inclusions. At that time, there were no competitors in the LREE uptake, suggesting that high LREE concentrations in apatite most probably are attributed to LREE enrichment in the melt. This is compatible with the predominance of mafic, LREE-rich and Mn-poor melt contribution in the earliest periods of the granodiorite formation. The second population of apatite, with lower LREE/Y and Na/Mn ratios, generated from a later, more equilibrated magma, which contained a larger contribution of a felsic melt.

Apatites from the RUD1, RUD2 and VRE granodiorites are positioned farthermost from the mafic end-member, however, the EM1/EM2 proportions are identical to those of some FOJ and MIL apatites. Nevertheless, the largest average EM1 contribution suggests that mixed and partially evolved magmas had already compositions shifted slightly towards the crustal end-member. This supposition is also supported by the relatively low apatite LREE/ Y ratios as well as Mn and Na contents slightly larger than in the early population of FOJ apatite. A larger contribution of a felsic magma might have 1) provided more Mn to be extracted from the melt by crystallizing apatite, 2) caused the shift in the preferred substitution mechanism from $LREE^{3+} + Si^{4+} \Leftrightarrow Ca^{2+} + P^{5+}$ to $HREE^{3+} + Na^{2+} \Leftrightarrow 2Ca^{2+}$, and 3) added more Al^{3+} to be coupled with Na^{+} (Sha and Chappell, 1999).

Large compositional diversity between apatites from individual granodiorites and potential end-members (EQU, LAM1, LAM2) allowed the PVA algorithm a clear distinction between each sample, generating a rock sequence that generally concords with the results of previous studies, but also addresses some new findings (e.g., position of the MIL granite). Unlike the whole-rock chemistry, only one felsic and one mafic end-member were detected, indicating that apatite did not record the heterogeneity of the mafic end-member and its evolution during the early stages of petrogenesis. On the other hand, the presence of EM2 points to potential participation of a fluid component enriched in trace elements. Relatively wide range of proportions of both felsic and mafic end-members in apatite

confirms the assumption that apatite crystallized in a complex magma mixing system composed of melt domains demonstrating a wide range of intermediate compositions.

6.4. Middle and late stages of magma evolution

During subsequent stages of magma evolution, a significant change in growth textures and composition of apatite occurred. Relatively homogenous, two-zoned (core and rim) or oscillatory zoned textures generally demonstrated by apatites from more evolved granite varieties indicate a more stable and undisturbed environment. Such textures suggest minor contribution of magma mixing on a local scale, caused by limited ability for mechanical mixing (difference in viscosity of coexisting melts) and decreased amounts of supplied mafic magma.

PVA apatite end-members calculated for middle and late stages are compositionally different from those of the early stage and show little systematic change over time. EM1 becomes slightly more enriched in LREEs, however, the change is insignificant. Increase in Mn content of EM1 from middle stage is consistent with progressive differentiation, however, its lower abundance in late-stage apatite is difficult to explain, giving that natural apatite from the late felsic rocks is most enriched in Mn. EM1 from the middle stage shows significant enrichment in Y, which is also reflected in apatite and whole-rock values and PVA whole-rock results. Higher Y results in lower LREE/Y ratios, which are indeed usually observed in apatites from middle and late stages (except for BUK and SOK). A more significant increase in Y content is observed in case of EM2, which is trace element-rich, similarly to the early stage. Enclaves are one of the most Y-rich rocks in the Karkonosze Massif, except of some composite dikes and equigranular granites. Such high Y signature cannot be the result of simple differentiation of the melt, as the opposite behaviour of Y is manifested from primitive to evolved rocks. The magmatic enclaves containing Y-rich apatite formed during middle-late stages of pluton formation and record multiple inflows of variably differentiated mafic melt. This diversity is seen in both whole-rock (Słaby and Martin, 2008) and apatite (slightly different composition between each enclave). High Y contents in apatites (and their host enclaves), as well as in EM2, point to the existence of a similar fluid phase (as in the early stage). This phase may represent an evolved mafic magma or a fluid exsolved from the evolved mafic melt. The presence of EM2 in the late stage and

high Y-contents in apatites from composite dikes are in accord with the documented fluid activity based on whole-rock composition of composite dikes (Słaby, 2006).

Detection of the mafic end-member (EM3) similar in composition to its equivalent from the early stage was possible due to selection of LAM1 apatites as a potential end-member. However, its PVA-generated chemistry is not reflected in apatites from the enclaves or composite dikes (especially the primitive ones - BUK and SOK). EM3 apatite is also depleted in LREEs and enriched in Si compared to apatite from the early stage, which is not consistent with the supposed coupled substitution mechanism $LREE^{3+} + Si^{4+} \Leftrightarrow Ca^{2+} + P^{5+}$. The elements which follow the typical differentiation process are F and Cl (F increases, while Cl decreases). Although the composition of EM2 slightly evolves from the early to late stage, its presence reflects mostly probably the same mechanisms as in the early stage.

Although not all porphyritic granites are included in PVA modelling (MICH is difficult to assign to a specific stage as it is younger than granodiorites and contains no enclaves or composite dikes), the evolution of apatite composition from primitive to evolved rocks is worth mentioning. The main parameter that changes during the progress of differentiation is the LREE/Y ratio, which is lowest in apatite from more evolved granites. If apatite is the only crystallizing LREE-bearing mineral, such modification is unlikely to be produced by fractional crystallization of one single magma, as both LREE and Y are incompatible elements and are concentrated in differentiated melts. Their melt−apatite partition coefficients increase by a similar rate with increasing polymerisation of the melt (Prowatke and Klemme, 2006), thus magma evolution would produce apatite with higher concentrations of LREEs and Y, but the ratio would remain relatively constant. However, the accessory mineral assemblage contains other LREE-bearing minerals, such as monazite and titanite. Titanite occurs in all Karkonosze granite varieties and demonstrates similar REE patterns as apatite. Monazite crystallized in more evolved rocks, i.e. moderately to evolved porphyritic granites. Even very small amounts of crystallizing monazite may affect the LREE budget and significantly decrease LREE uptake by apatite (Förster, 1999; Förster and Rhede, 2005). Therefore, lower LREE/Y ratios can be partially due to monazite appearance (xenotime is absent). However, a second explanation for the decrease of LREE/Y ratios in apatite can be given. Decreasing amounts of supplied LREE-rich

mafic magma and, consequently, higher contribution of the Y-richer felsic melt, could be responsible for the transition in apatite LREE/Y ratios. As both mentioned explanations are plausible, we conclude that, most probably, they both contributed to the shift in LREE and Y contents in apatite. Abundance of Cl in apatite decreases during differentiation, also reflecting diminishing role of the mafic magma.

Although apatites from different enclaves, composite dikes and porphyritic granites exhibit some compositional differences (e.g., LREE/Y ratio, contents of Mn, Na, Cl and Sr) suggesting different degree of evolution and proportions of coeval magmas, such diversity is not observed in the end-member proportion diagrams (Figs. 9, 10). As the mafic apatite end-member (calculated based on the LAM1 apatite) has a composition distinct even from apatite from more primitive enclaves and composite dikes, all apatites are positioned far from the EM3 vertex and very close to the felsic end-member. The difference in the position of LAM1 apatites on ternary plots between the middle and late stages may be explained by the fact that this lamprophyre is most compatible in composition with the most evolved mafic end-member. There is no distinction between apatites from individual enclaves and, moreover, between the apatites from the enclaves and their granite host. Similar situation is observed for the late-stage granites and composite dikes. The close affinity between enclave and EQU apatites may be attributed to the choose of LAM1 apatite as potential end-member. Enclave apatites are compositionally very distinct from the LAM1 apatites, thus, they are located distant from them on the proportion diagram. However, this position may have also a petrogenetical background. Studied mafic enclaves are hybrids which underwent 1) evolution by fractional crystallization of the mafic end-member, 2) minor mechanical mixing (reduced mixing capability owing to greater abundance of crystals and, thus, viscosity of both magmas; Davi et al., 2009), but possibly intensive chemical exchange with the host, and 3) potential interaction with fluids (Adamuszek et al., 2009; Słaby and Martin, 2008; Słaby et al., 2008). Perhaps the combination of these processes resulted in the formation of apatite already bearing a more felsic signature. Adamuszek et al. (2009) documented that diffusion of elements between the enclave and its host may be enhanced in case of mobile elements, especially in the presence of fluids. In such situation, the concentrations of those elements in the enclave may reach similar levels as in their host, controlling the uptake of trace elements by apatite. Similar

assumption was made by Liu et al. (2013), who documented re-equilibration between a mafic enclave and its host, resulting in similar trace-element and isotopic compositions.

The distribution of apatite from composite dikes on the proportion diagram of the late stage can be adequately explained. During ascent of a dike, chemical exchange will be promoted at the contact with the host rocks (in this case the equigranular granite), even though the mechanical mixing is limited due to difference in viscosity (low viscosity of a dike vs. partial solidification of the granite). Therefore, re-equilibration may have caused the compositional similarity between apatites from the composite dikes and equigranular granite and, hence, their position far from the mafic end-member (EM3) in the PVA diagram. Higher contribution of EM2 suggests most probably a more dominant role of Y- and Si-rich fluids in the late stage, thus supporting previous studies (Słaby, 2006).

Based on the PVA diagrams, the evolution of the Karkonosze magmatic system can be characterized by progressive homogenization of the two distinct magmas, with diminishing role of the mafic component during time. During the early stages, the compositional diversity is greatest, whereas in the course of differentiation, the range gets smaller and differences between individual rocks become less striking (however still present). The same path is documented in apatite. A change from a largely scattering distribution from the early stage to very narrow clustering in the middle and late stages on the PVA diagram may represent exactly such homogenization of the system, where apatite becomes compositionally less diverse.

6.5. Limitations of the PVA method applied for mineral compositions

Whereas whole-rock composition is the overall effect of the combination of all processes operating during magmatic evolution, the composition of a single mineral is only one part of the system, controlled by numerous factors (cf. section 6.2). Although studied apatites reflect the magma chemistry quite well, the use of apatite composition as input data for PVA may pose problems, some of which are reflected in the results of this study. As unusual enrichments in trace elements (e.g. REE, Y, Si) can be related to supersaturation, the PVA-generated end-members with high concentrations of these elements do not properly reflect the intensity of enrichments in the magma/fluid. The PVA-inferred chemistry ofEM2 apatite is an expression of this problem. However, it is unlikely that a large number of apatites crystallized at supersaturation conditions, therefore, a fluid affinity of EM2 is more

plausible. Diffusive fractionation may also disturb the relations between whole-rock and apatite chemistry and result in different elemental ratios in some apatite domains, which, in turn, may yield not entirely true end-members.

The group of elements incorporated in apatite showing the widest spread in concentrations, even in single samples, are REEs. Although average REE content may be lower in few samples (e.g. LAM1, LAM2, EQU), the bulk of apatite analyses shows similar average REE concentrations. Nevertheless, there exist apatite zones with exceptionally high or low REE contents. This circumstance hinders the appropriate subdivision of REEs between the end-members, probably giving rise to the generation of REE-free EM1 and REE-rich EM2. REE content also depends on the melt/apatite partition coefficient (K_d), which increases with progressive differentiation of the melt (Prowatke and Klemme, 2003). Following that rule, K_d for the apatite/lamprophyre system is lower than K_d for apatite/granite. Consequently, even though lamprophyres in Karkonosze are REE-enriched relative to granites, apatites from the latter will incorporate larger REE concentrations. The corresponding end-members may, therefore, show REE contents inconsistent with real enrichments or depletions in the melt.

Important in PVA simulations is also the choice of potential end-members. In current runs, equigranular granite and lamprophyre served as potential parental magmas. Apatite from the lamprophyre has extreme composition in terms of halogens, Sr and S. Whereas in the early stage, apatites from the granodiorites and MIL sample show some affinity to EM3 (and, therefore, display a relatively wide spread between EM1 and EM3), apatites from the enclaves or composite dikes have more uniform chemistry, which is closer to the felsic end-member. As it probably represents the progressive homogenization of the system resulting in a narrower range of apatite compositions, the absence of apatites with higher contribution of EM3 in the middle and late stages may be related to the choice of the extreme LAM1 apatites as potential end-member. LAM1 apatites may not be fully representative of the pure mafic end-member from these stages (as no real representative exists) and, therefore, their composition could only be judged as approximation. Methodologically, PVA requires also significant variations in elemental concentrations and, preferably, a large compositional spread of samples between potential end-members (presence of samples with low and high proportions of each end-member). Therefore, the early stage of magma evolution gave results most compatible with

previous studies, as the compositional variations between apatites from granodiorites and their similarity to end-member were the greatest. In subsequent stages, the differences in chemistry were too subtle and too distinct from the chemically extreme LAM1 apatite.

7. Summary and conclusions

1. PVA of whole-rock composition yielded results that confirm the present general geological model developed for the Karkonosze batholith, but also provided some new aspects. Apart from supporting the idea of mixing (+ FC) between the felsic and mafic end-members, PVA revealed that the diversity among granodiorites and magmatic enclaves resulted mostly from the evolution of the mafic end-member, and not only different proportions of felsic vs. mafic magma as suggested by previous studies. Additionally, PVA recognized the addition of a fluid component probably derived from the metasomatized mantle.
2. Using minerals as proxies of magma compositions is problematic owing to many factors that control their composition. Some features of the studied apatite (e.g., unusual enrichment in certain elements) may not properly reflect the magma chemistry, as it can also be a result of supersaturation or diffusive fractionation. However, the apatite studied here follow the general evolution of the magma chemistry quite well, therefore, their use for PVA modelling is justified.
3. Apatite end-members generated by PVA are mostly compatible with the whole-rock chemistry and real apatite composition. Recognized end-members include felsic, mafic and fluid components, however, not all of them are present in every sample. Large compositional diversity between apatites from the early-stage samples allowed a clear distinction between each sample, presenting a rock sequence which is in accord with previous studies. Wide range of proportions of felsic and mafic end-members in early-stage apatite gives evidence of its crystallization within a complex magma mixing system composed of melt domains of contrasting compositions. Additionally, the presence of a fluid component associated with the mafic magma was recognized.

4. In the middle and late stages, apatites display a more uniform composition and a narrow range of end-member proportions, most probably reflecting a progressive homogenization of the system. PVA results enabled the recognition of fluid activity during the middle stages, which is most prominent in apatite crystallization compared to early and late stages.
5. The application of mineral compositions in PVA modelling is conflicted with some limitations, both due to the method itself and the fact, that mineral chemistry may not fully reflect that of the magma from which it crystallized. However, if the chemical composition of a mineral is recognized and assigned to particular processes and all the limitations are taken into account, PVA modelling of single-mineral composition may give rise to a more detailed image of the magmatic evolution at local scale and stage by stage.

Acknowledgements

We thank Dieter Rhede (GFZ) for his assistance with the electron-microprobe measurements. We are indebted to T. A. Vogel and I. Broska for their constructive and thought-provoking reviews. T. A. Vogel is especially acknowledged for sharing his PVA software with us. This study was supported by a NCN grant 2011/01/N/ST10/04756 and ING PAN "Lotny".

References

Adamuszek, M., John, T., Dabrowski, M., Podladchikov, Y. Y., Gertisser, R., 2009. Assimilation and diffusion during xenolith-magma interaction: a case study of the Variscan Karkonosze Granite, Bohemian Massif. Mineralogy and Petrology 97, 203-222.

Armstrong, J.T., 1995. CITZAF: a package of correction programs for the quantitative electron microbeam X-ray-analysis of thick polished materials, thin films, and particles. Microbeam Analysis 4, 177–200.

Awdankiewicz, M., Awdankiewicz, H., Kryza, R., 2005. Petrology of mafic and felsic dikes from the eastern part of the Karkonosze massif. Polish Mineralogical Society, Special Papers 26, 111-114.

Awdankiewicz, M., 2007. Late Palaeozoic lamprophyres and associated mafic subvolcanic rocks of the Sudetes (SW Poland): petrology, geochemistry and petrogenesis. Geologia Sudetica 39, 11-97.

Barbarin, B., 1999. A review of the relationships between granitoid types, their origins and their geodynamic environments. Lithos 46, 605-626.

Barbarin, B., 2005. Mafic magmatic enclaves and mafic rocks associated with some granitoids of the central Sierra Nevada batholith, California: nature, origin, and relations with the hosts. Lithos 80, 155-177.

Barclay, J., Herd, R. A., Edwards, B., Kiddle, E., Donovan, A., 2010. Caught in the act: Implications for the increasing abundance of mafic enclaves during the eruption of the Soufriere Hills Volcano, Montserrat. Geophysical Research Letters, 37.

Belousova, E.A., Griffin, W.L., O'Reilly, S. Y., Fisher, N.I., 2002. Apatite as an indicator mineral for mineral exploration: trace-element compositions and their relationship to host rock type. Journal of Geochemical Exploration 76, 45-69.

Borkowska, M., 1966. Petrography of Karkonosze granite. Geologia Sudetica 2, 7-119.

Boyce, J.W., Hervig, R.L., 2009. Apatite as a monitor of late-stage magmatic processes at Volcán Irazú, Costa Rica. Contributions to Mineralogy and Petrology 157, 135-145.

Buda, G., Pal-Molnar, E. 2012. Apatite as a petrogenetic indicator of Variscan granitoids in Tisza mega-unit (South Hungary). Carpathian Journal of Earth and Environmental Sciences 7, 47-60.

Chu, M., Wang, K., Griffin, W., Chung, S., O'Reilly, S., Pearson, N., Iizuka, Y., 2009. Apatite Composition: Tracing Petrogenetic Processes in Transhimalayan Granitoids. Journal of Petrology 50, 1829–1855.

De Campos, C.P., Dingwell, D.B., Perugini, D., Civetta, L., Fehr, T.K., 2008. Heterogeneities in magma chambers: insights from the behavior of major and minor elements during mixing experiments with natural alkaline melts. Chemical Geology 256, 131–145.

De Campos, C. P., Perugini, D., Ertel-Ingrisch, W., Dingwell, D. B., Poli, G., 2011. Enhancement of magma mixing efficiency by chaotic dynamics: an experimental study. Contributions to Mineralogy and Petrology 161, 863–881.

Davì, M., Behrens, H., Vetere, B., De Rosa, R., 2009. The viscosity of latitic melts from Lipari (Aeolian Islands, Italy): Inference on mixing–mingling processes in magmas. Chemical Geology 259, 89-97.

Deering, C. D., Cole, J. W., Vogel, T. A., 2008. A rhyolite compositional continuum governed by lower crustal source conditions in the Taupo Volcanic Zone, New Zealand. Journal of Petrology 49, 2245-2276.

Dempster, T. J., Jolivet, M., Tubrett, M. N., Braithwaite, C. J. R., 2003. Magmatic zoning in apatite: a monitor of porosity and permeability change in granites. Contributions to Mineralogy and Petrology 145, 568-577.

Dokuz, A., 2011. A slab detachment and delamination model for the generation of Carboniferous high-potassium I-type magmatism in the Eastern Pontides, NE Turkey: The Köse composite pluton. Gondwana Research 19, 926–944.

Förster, H.-J., 1999. The chemical composition of uraninite in Variscan granites of the Erzgebirge, Germany. Mineralogical Magazine 63, 239–252.

Förster, H.-J., Rhede, D., 2006. The Be–Ta-rich granite of Seiffen (eastern Erzgebirge, Germany): accessory-mineral chemistry, composition, and age of a post-collisional Li–F granite of A-type affinity. Neues Jahrbuch Mineralogie Abhandlungen 183, 307–321.

Fourcade, S., Allégre, C. J., 1981. Trace element behaviour in granite genesis: a case study. The calc-alkaline plutonic association from Querigut complex (Pyrenees, France). Contributions to Mineralogy and Petrology 76, 177-195.

Fujimaki, H., 1986. Partition-coefficients of Hf, Zr, and REE between zircon, apatite, and liquid. Contributions to Mineralogy and Petrology 94, 42-45.

Gourgaud, A., Villemant., B., 1992. Evolution of magma mixing in an alkaline suite: the Grande Cascade sequence (Monts-Dore, French Massif Central). Geochemical modelling. Journal of Volcanology and Geothermal Research 52, 255-275.

Janoušek, V., Braithwaite, C. J. R., Bowes, D. R., Gerdes, A., 2004. Magma-mixing in the genesis of Hercynian calc-alkaline granitoids: an integrated petrographic and geochemical study of the Sazava intrusion, Central Bohemian Pluton, Czech Republic. Lithos 78, 67-99.

Johnson, G.W., Ehrlich, R., Full, W., 2001. Principal components analysis and receptor models in environmental forensics. In: Murphy, B.L., Morrison, D. (Eds), Introduction to environmental forensics.Klominsky, J., 1969. Krkonossko-jizersky granitoid massif. Sbornik GeologickichVed, Geologie 15, 7-132.

Kusiak, M. A., Dunkley, D. J., Słaby, E., Budzyń, B., Martin, H., 2008a. U–Pb chronology of zircon from granites of the Karkonosze Pluton, NE Bohemian Massif. 4th SHRIMP workshop, Saint Petersburg, Russia, Abstract Volume, pp. 70–80.

Kusiak, M. A., Dunkley, D. J., Słaby, E., Budzyń, B., Martin, H., 2008b. Metasomatized zircon in equigranular granite from the Karkonosze Pluton, NE Bohemian Massif. In: Harlov, D., Broska, I. (Eds), Mineral Equilibria, Metasomatism and Mass Transport: Evolution and Stabilisation of Rock on a Fluid-Rich World. Proceedings from MIMET 2008 Workshop, Smolenice, Slovak Republic, April 8– 10 (eds), pp. 87–90.

Kusiak, M. A., Williams, I. S., Dunkley, D. J., Konečny, P., Słaby, E., Martin, H., 2014. Monazite to the rescue: U-Th-Pb dating of the intrusive history of the composite Karkonosze pluton, Bohemian Massif. Chemical Geology 364, 76-92.

Liu, L., Qiu, J.-S., Li, Z., 2013. Origin of mafic microgranular enclaves (MMEs) and their host quartz monzonites from the Muchen pluton in Zhejiang Province, Southeast China: Implications for magma mixing and crust–mantle interaction. Lithos 160-161, 145-163.

Machowiak, K., Armstrong, R., 2007. SHRIMP U–Pb zircon age from the Karkonosze granite. Mineralogia Polonica, Special Papers 31, 193–196.

Marks, M. A.W., Wenzel, T., Whitehouse, M. J., Loose, M., Zack, T., Barth, M., Worgard, L., Krasz, V., Eby, G. N., Stosnach, H., Markl, G., 2012. The volatile inventory (F, Cl, Br, S, C) of magmatic apatite: An integrated analytical approach. Chemical Geology 291, 241-255.

Martins, H.C.B., Sant'Ovaia, H., Noronha, F., 2013. Late-Variscan emplacement and genesis of the Vieira do Minho composite pluton, Central Iberian Zone: Constraints from U-Pb zircon geochronology, AMS data and Sr–Nd–dicron geochronology, Lithos 162-163, 221-235.

Mazur, S., Aleksandrowski, P., 2001. The Tepla(?)/Saxothuringian suture in the Karkonosz-Izera Massif, western Sudetes, Central European Variscides. International Journal of Earth Sciences 90, 341-360.

Mierzejewski, M. P., Oberc, D. T., 1990. The Izera-Karkonosze Block and its tectonic development (Sudetes, Poland). Neues Jahrbuch für Geologie und Paläontologie, Abhandlungen 179, 197-222.

Morgavi, D., Perugini, D., De Campos, C. P., Ertel-Ingrisch, W., Lavall´ee, Y., Morgan, L., Dingwell, D. B., 2013a. Interactions between rhyolitic and basaltic melts unraveled by chaotic mixing experiments. Chemical Geology 346, 192-212.

Morgavi, D., Perugini, D., De Campos, C. P., Ertel-Ingrisch, W., Dingwell, D. B., 2013b. Time evolution of chemical exchanges during mixing of rhyolitic and basaltic melts. Contributions to Mineralogy and Petrology 166, 615-638.

O'Reilly, S. Y., Griffin, W. L., 2000. Apatite in the mantle: implications for metasomatic processes and high heat production in Phanerozoic mantle. Lithos 53, 217-232.

Patočka, F., Fajst, M., Kachlik, V., 2000. Mafic, felsic to mafic-ultramafic Early Palaeozoic magmatism of the West Sudetes (NE Bohemian Massif): the South Krkonosze complex. Zeitschrift für Geologische Wissenschaften 28, 177-210.

Patiño Douce, A. E., Roden, M. F., Chaumba, J., Fleisher, C., Yogodzinski, G., 2011. Compositional variability of terrestrial mantle apatites, thermodynamic modeling of apatite volatile contents, and the halogen and water budgets of planetary mantles. Chemical Geology 288, 14-31.

Perugini, D., Poli, G., 2012. The mixing of magmas in plutonic and volcanic environments: Analogies and differences. Lithos 153, 261-277.

Perugini, D., Poli, G., Mazzuoli, R., 2003. Chaotic advection, fractals and diffusion during mixing of magmas: evidence from lava flows. Journal of Volcanology and Geothermal Research 124, 255–279.

Perugini, D., Petrelli, M., Poli, G., 2006. Diffusive fractionation of trace elements by chaotic mixing of magmas. Earth and Planetary Science Letters 243, 669–680.

Perugini, D., De Campos, C.R., Dingwell, D.B., Petrelli, M., Poli, G., 2008. Trace element mobility during magma mixing: preliminary experimental results. Chemical Geology 256, 146–157.

Perugini, D., De Campos, C.P., Ertel-Ingrisch, W., Dingwell, D.B., 2012. The space and time complexity of chaotic mixing of silicate melts: Implications for igneous petrology. Lithos 155, 326-340.

Perugini, D., De Campos, C.P., Dingwell, D.B., Dorfman, A., 2013. Relaxation of concentration variance : A new tool to measure chemical element mobility during mixing of magmas. Chemical Geology 335, 8-23.

Pin, C., Mierzejewski, P. M., Duthou, J. L., 1987. Isochronous age Rb/Sr of Karkonosze granite from the quarry Szklarska Poręba Huta and significance of initial ratio 87Sr/86Sr in this granite. Przegląd Geologiczny 35, 512-516.

Prowatke, S., Klemme, S., 2006. Trace element partitioning between apatite and silicate melts. Geochimica et Cosmochimica Acta 70, 4513-4527.

Przywóski, L., 2006. Chemical and CL study on apatite as an indicator of Karkonosze granite petrogenesis. MSc thesis, University of Warsaw.

Rollinson, H. R., 1993. Using geochemical data: Evaluation, Presentation, Interpretation. Longman Scientific & Technical, London.

Sha, L.-K., Chappell, B.W., 1999. Apatite chemical composition, determined by electron microprobe and laser-ablation inductively coupled plasma mass spectrometry, as a probe into granite petrogenesis. Geochimica et Cosmochimica Acta 63, 3861–3881.

Słaby, E., 2005. CHARAC- non-CHARAC behaviour of Y/Ho and Zr/ Hf in Karkonosze hybridic and granitic melts. Polish Mineralogical Society, Special Papers 25, 200–203.

Słaby, E., 2006. Record of magma differentiation in apatite from Karkonosze hybrids – preliminary results. Mineralogical Society of Poland, Special Papers 29, 196-199.

Słaby, E., Götze, J., 2004. Feldspar crystallization under magma mixing conditions shown by cathodoluminescence and geochemical modelling: case study from the Karkonosze pluton (SW Poland). Mineralogical Magazine 68, 541-557.

Słaby, E., Martin, H., 2005. Mechanisms of differentiation of the Karkonosze granite. Mineralogical Society of Poland, Special Papers 26, 264-267.

Słaby, E., Martin, H., 2008. Mafic and felsic magma interaction in granites: the Hercynian Karkonosze Pluton (Sudetes, Bohemian Massif). Journal of Petrology 49, 353-391.

Słaby, E., Galbarczyk-Gąsiorowska, L., Baszkiewicz, A., 2002. Mantled alkali-feldspar megacrysts from the marginal part of the Karkonosze granitoid massif (SW Poland). Acta Geologica Polonica 52, 501-519.

Słaby, E., Galbarczyk-Gąsiorowska, L., Seltmann, R., Müller, A., 2007a. Alkali feldspar megacryst growth: geochemical modelling. Mineralogy and Petrology 68, 1–29.

Słaby, E., Seltmann, R., Kober, B., Müller, A., Galbarczyk-Gąsiorowska, L., Jeffries, T., 2007b. LREE distribution patterns in zoned alkali feldspar megacrysts −implication for parental melt composition. Mineralogical Magazine 71, 193–217.

Słaby, E., Götze, J., Wörner, G., Simon, K., Wrzalik, R., Śmigielski, M., 2008. K-feldspar phenocrysts in microgranular magmatic enclaves: a cathodoluminescence and geochemical study of crystal growth as a marker of magma mingling dynamics. Lithos 105, 85–97.

Słaby, E., Śmigielski, M., Domonik, A., Simon, K., Kronz, A., 2011. Chaotic three-dimensional distribution of Ba, Rb and Sr in feldspar megacrysts grown in an open magmatic system. Contributions to Mineralogy and Petrology 162, 909-927.

Słaby, E., Martin, H., Hamada, M., Śmigielski, M., Domonik, A., Götze, J., Hoefs, J., Hałas, S., Simon, K., Devidal, J.-L., Moyen, J.-F., Jayananda, M., 2012. Evidence in Archaean alkali feldspar megacrysts for high-temperature interaction with mantle fluids. Journal of Petrology 53, 67-98.

Spicer, E., Scheepers, R., Miller, J. 2006. Apatite, allanite and monazite as petrogenetic indicators in S-, I- and A-type granites of the Cape Granite Suite, Western Cape Province, South Africa. Geophysical Research Abstracts 8, 06363.

Szopa, K., Gawęda, A., Müller, A., Sikorska, M., 2013. The petrogenesis of granitoid rocks unusually rich in apatite in the Western Tatra Mts. (S-Poland, Western Carpathians). Mineralogy and Petrology 109, 609-627.

Szymanski, D.W., Patino, L.C., Vogel, T.A., Alvarado, G.E., 2013. Evaluating complex magma mixing via Polytopic Vector Analysis (PVA) in the Papagayo Tuff, Northern Costa Rica: processes that form continental crust. Geosciences 3, 585-615.

Tefend, K. S., Vogel, T. A., Flood, T. P., Ehrlich, R., 2007. Identifying relationships among silicic magma batches by polytopic vector analysis: A study of the Topopah Spring and Pah Canyon ash-flow sheets of the southwest Nevada volcanic field, Journal of Volcanology and Geothermal Research 167, 198–211.

Vogel, T. A., Hidalgo, P. J., Patino, L., Tefend, K. S.,. Ehrlich, R., 2008. Evaluation of magma mixing and fractional crystallization using whole- rock chemical analyses: Polytopic vector analyses, Geochemistry, Geophysics, Geosystems 9, Q04020, doi:10.1029/2007GC001790.

Watson, E.B., Green, T.H., 1981. Apatite/liquid partition coefficients for the rare earth elements and strontium. Earth and Planetary Science Letters 56, 405-421.

Wilamowski, A., 1998. Środowisko geotektoniczne intruzji granitowych Tatr i Karkonoszy w świetle danych geochemicznych. Archiwum Mineralogiczne 52, 261-271.

Žák, J., Vyhnalek, B., Kabele, P., 2006. Is there a relationship between magmatic fabrics and brittle fractures in plutons? A view based on structural analysis, anisotropy of magnetic susceptibility and thermo-mechanical modelling of the Tanvald pluton (Bohemian Massif). Physics of the Earth and Planetary Interiors 157, 286-310.

Žák, J., Klominsky, J., 2007. Magmatic structures in the Krkonoše-Jizera Plutonic Complex, Bohemian Massif: evidence for localized multiphase flow and small-scale thermal-mechanical instabilities in a granitic magma chamber. Journal of Volcanology and Geothermal Research 164, 254-267.

Žák, J., Verner, K., Sláma, J., Kachlík, V., Chlupáčová, M., 2013. Multistage magma emplacement and progressive strain accumulation in the Krkonoše–Jizera plutonic complex, Bohemian Massif. Tectonics 32, 1493–1512.

Figure captions

Fig.1. Simplified geological map of the study area (after Patočka et al. 2000). IG –Izera gneisses and granito-gneisses with belts of mica schists; EKC - Eastern Karkonosze Complex; LV -Leszczyniec unit; SKC - Southern Karkonosze Complex. Geographical coordinates of the sampling sites are given in Table 1.

Fig.2. Back-scattered electron (BSE) images of representative apatite grains from granodiorites and primitive porphyritic granite; a – apatite grain from the FOJ granodiorite, hosted in biotite; b – apatite grain from the FOJ grain mount; c − apatite grain from the RUD1 granodiorite, hosted in feldspar, electron microprobe data for the marked spots are given in Table S8 – Supplementary Electronic Material; d – apatite grain from the MIL porphyritic granite, attached to biotite.

Fig.3. BSE images of representative apatite grains from porphyritic granites, magmatic enclaves and composite dikes; a – apatite grain from the MICH grain mount; b – apatite grain from the SPH grain mount; c – apatite grain from the ENK3 grain mount; d − apatite grain from the BUK enclave, hosted in biotite; e – apatite grain from the SOK grain mount; f – apatite grain from the EQU sample, hosted in biotite.

Fig.4. ΣLREE vs. Y plots for apatite from all studied samples; a – for apatites insideand outside of biotite in FOJ granodiorite; b – for apatites from remaining granodiorites; c – for apatites from primitive and evolved porphyritic granites; d – for apatites from magmatic enclaves; e – for apatites from composite dikes;

Fig.5. Mn vs. Na plots for apatite from all studies samples; a – for apatites inside and outside of biotite in FOJ granodiorite; b – for apatites from remaining granodiorites; c - for apatites from composite dikes; d - for apatites from magmatic enclaves; e - for apatites from primitive and evolved porphyritic granites.

Fig.6. F vs. Cl plots for apatites from all studies samples; a – for apatites from all granodiorites (EQU excluded); b – for apatites from the FOJ granodiorite and MIL porphyritic granite (LAM1 excluded); c – for apatites from the porphyritic granites (LAM1 and LAM2 excluded); d – for apatites from magmatic enclaves (LAM1 and LAM2 excluded); e – for apatites from the composite dikes (LAM1 and LAM2 excluded).

Fig.7. Proportion diagram of a three end-member solution for the run Whole-rock All; EM1 – felsic end-member; EM2 and EM3 – mafic end-members;

Fig.8. Proportion diagram of a three end-member solution for the run Apatite Early Stage; EM1 – felsic end-member, EM2 – potential fluid component, EM3 – mafic end-member; a – points representing all measured apatite zones; b – simplified plot with marked areas for each sample.

Fig.9. Proportion diagram of a three end-member solution for the run Apatite Middle Stage; EM1 – felsic end-member, EM2 – potential fluid component, EM3 – mafic end-member; a – points representing all measured apatite zones; b – simplified plot with marked areas for each sample.

Fig.10. Proportion diagram of a three end-member solution for the run Apatite Late Stage; EM1 – felsic end-member, EM2 – potential fluid component, EM3 – mafic end-member.

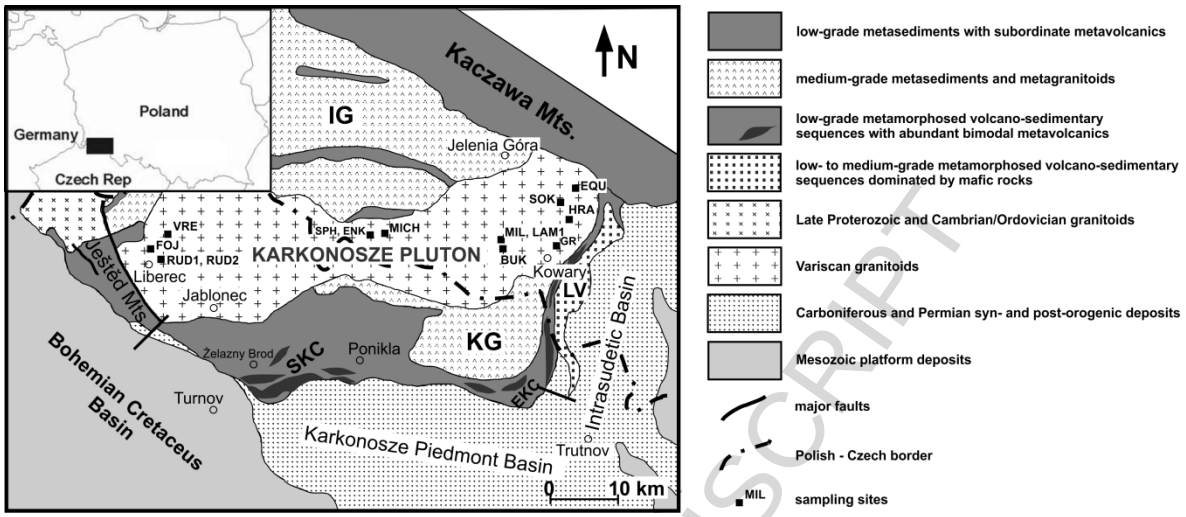

Figure 1

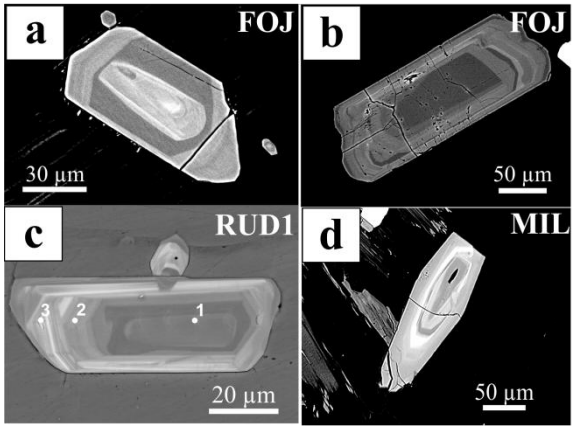

Figure 2

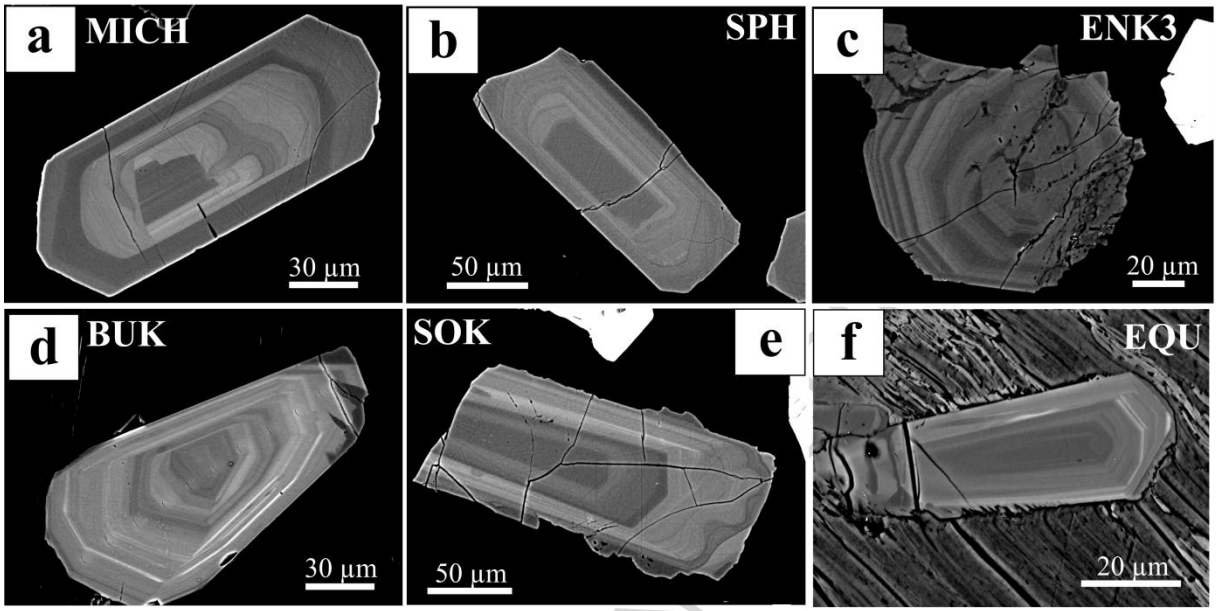

Figure 3

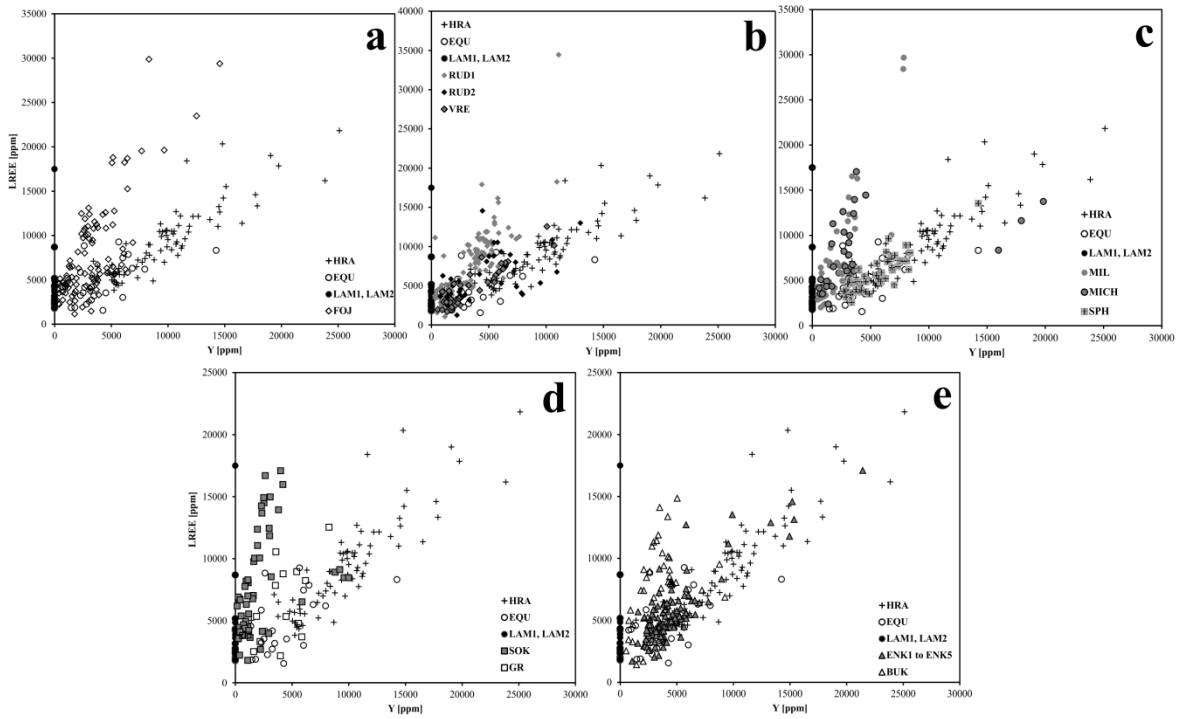

Figure 4

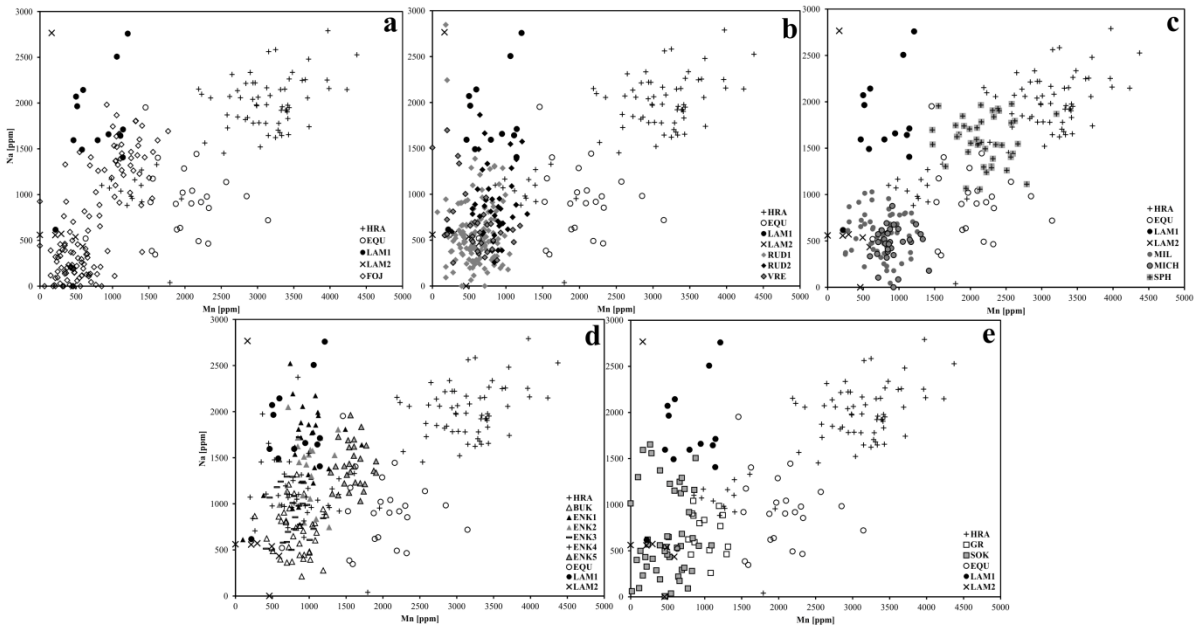

Figure 5

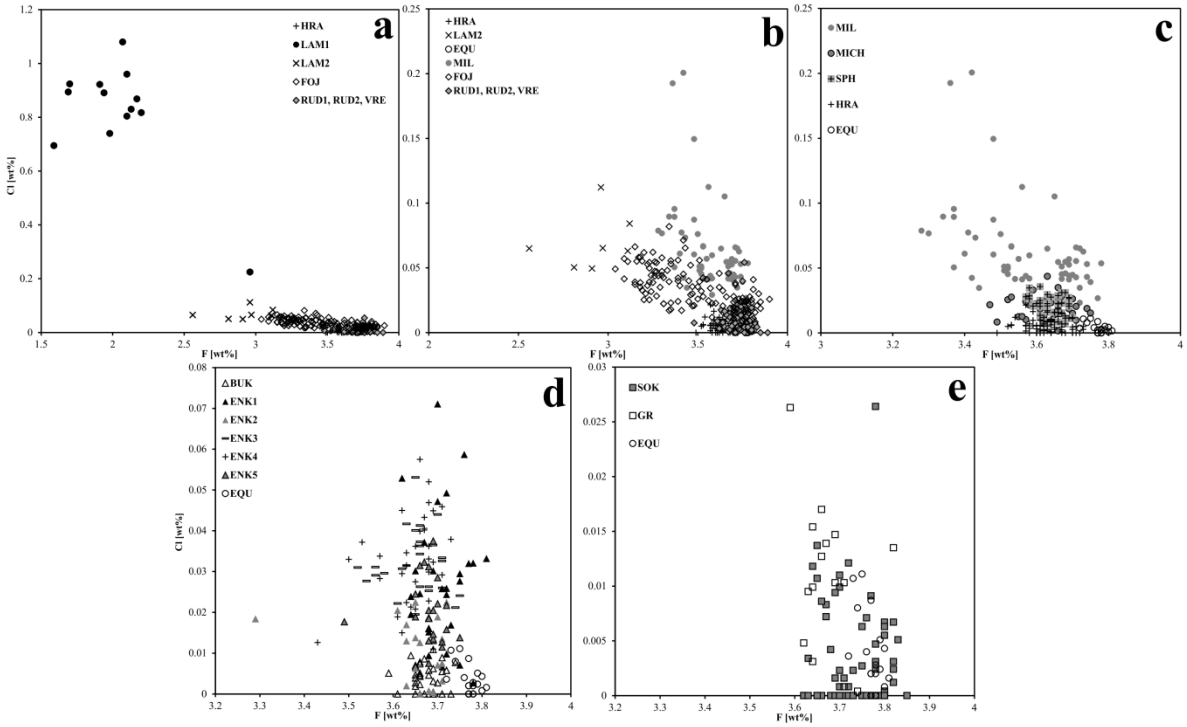

Figure 6

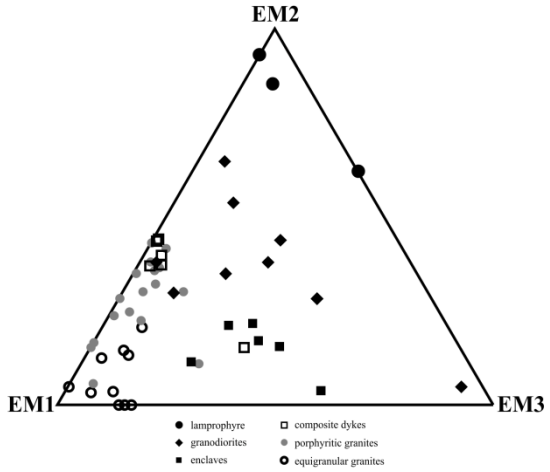

Figure 7

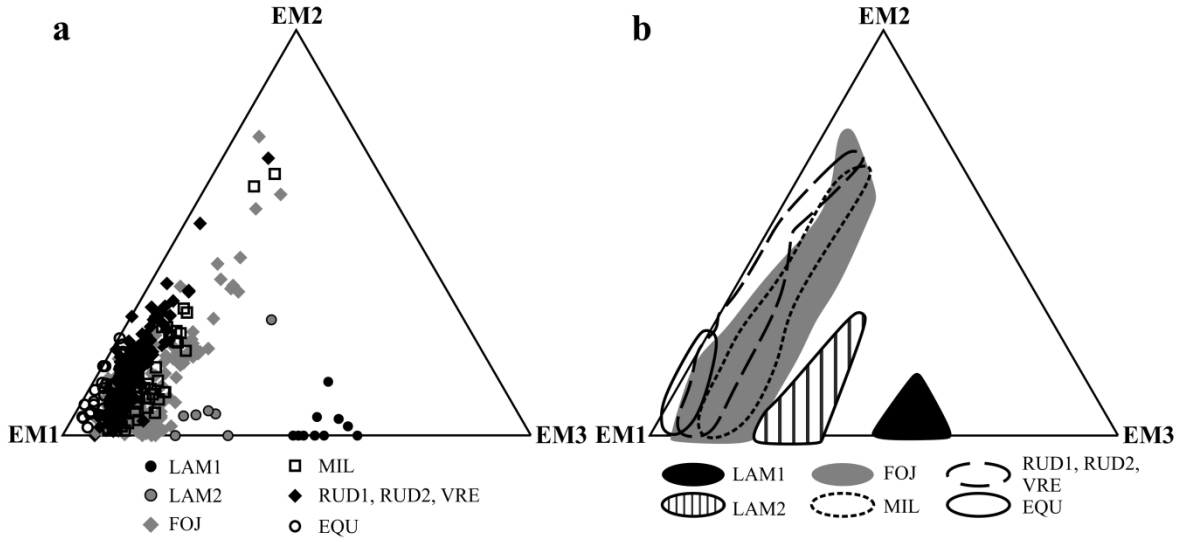

Figure 8

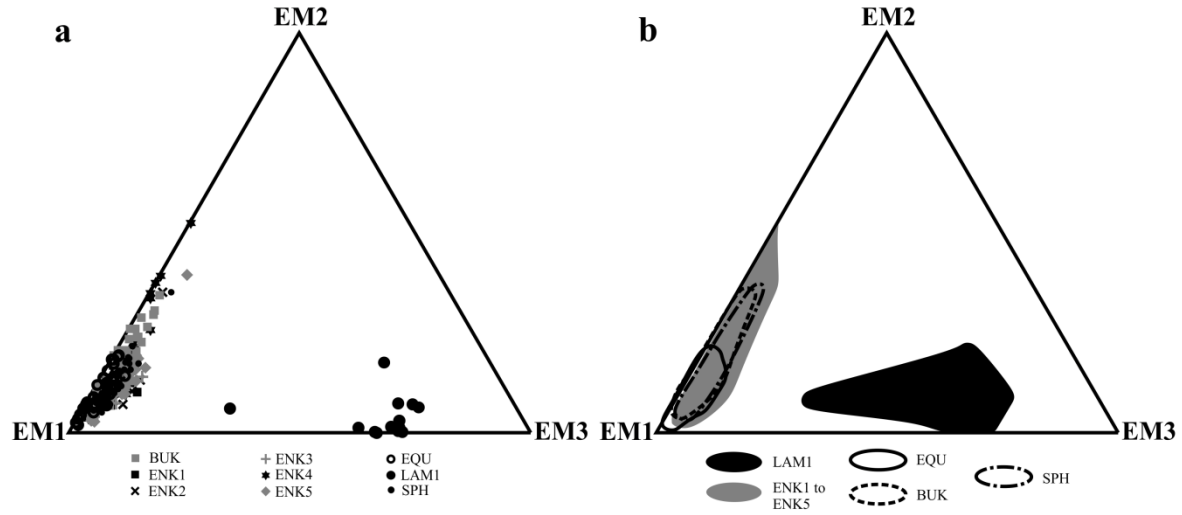

Figure 9

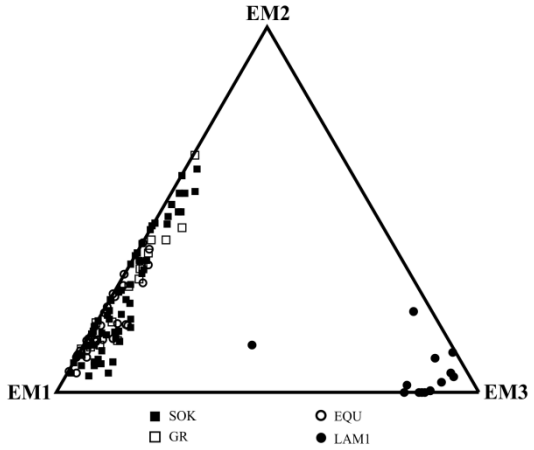

Figure 10

Table 1. Localization of the studied samples.

Sample name	Rock type	Localization	Coordinates
LAM1 *(LAM4)*[1]	lamprophyre	Karpacz	50°49'N 15°46'E
LAM2	lamprophyre	Bukowiec	Unknown
FOJ *(HYB8)*	homogeneous granodiorite	Fojtka	50°50'N 15°04'E
RUD1 *(HYB10)*	heterogeneous granodiorite	Rudolfov	50°47'N 15°06'E
RUD2 *(HYB11)*	heterogeneous granodiorite	Rudolfov	50°47'N 15°06'E
VRE *(HYB12)*	heterogeneous granodiorite	Vresoviste	50°50'N 15°05'E
MIL *(POR6)*	primitive porphyritic granite	Miłków	50°49'N 15°46'E
MICH *(POR10)*	slightly evolved porphyritic granite	Michałowice	50°50'N 15°34'E
SPH *(POR26)*	evolved porphyritic granite	Szklarska Poręba-Huta	50°50'N 15°29'E
BUK *(MME6)*	dark enclave	Bukówka	50°48'N 15°46'E
ENK1 to ENK5	moderately dark enclaves	Szklarska Poręba-Huta	50°50'N 15°29'E
SOK *(COM4)*	composite dyke	Sokoliki	50°52'N 15°52'E
GR *(COM5)*	composite dyke	Gruszków	50°49'N 15°51'E
HRA *(EQU1)*	less evolved equigranular granite	Hraniczna	50°50'N 15°55'E
EQU *(EQU15)*	most evolved equigranular granite	Sokoliki	50°52'N 15°52'E

[1]*(LAM4)* - Acronyms of corresponding rocks from Słaby and Martin (2008)

Table 2. Analytical conditions of the electron microprobe measurements.

Element	X-ray line	Standard	Crystal	Counting time (s)	Detection limit (1σ) (ppm)
F	Ka	CaF2	LDE1	10	470
Na	Ka	Albite	TAP	10	270
Mg	Ka	Periclase	TAP	20	110
Al	Ka	Orthoclase	TAP	20	110
Si	Ka	Orthoclase	TAP	10	230
P	Ka	Apatite	PET	10	260
S	Ka	Sphalerite	PET	20	190
Cl	Ka	Tugtupite	PET	20	80
Ca	Ka	Apatite	PETH	10	90
Mn	Ka	Rhodonite	LiF	20	200
Fe	Ka	Hematite	LiF	20	190
Sr	La	Celestine	TAP	20	320
Y	La	YPO4	TAP	50	180
La	La	LaPO4	LiF	50	470
Ce	La	CePO4	LiF	50	410
Pr	Lb	PrPO4	LiF	50	530
Nd	Lb	NdPO4	LiF	50	480
Sm	Lb	SmPO4	LiF	50	480
Gd	Lb	GdPO4	LiF	50	480
Dy	Lb	DyPO4	LiF	50	500
Er	Lb	ErPO4	LiF	50	530
Yb	La	YbPO4	LiF	50	260
Th	Ma	Th-metal	PETH	50	110
U	Mb	U-metal	PETH	50	160

Table 3. Description of type and number of samples used for each PVA simulation.

Run	Composition	Number of samples/grains/analyses used	Sample list	Number of generated end-members	Method of primary polytope initialization
Whole-rock All	Whole-rock	51	10 samples of equigranular granite, 17 samples of porphyritic granite, 3 samples of lamprophyre, 9 samples of granodiorite, 6 samples of magmatic enclaves, 6 samples of composite dykes	3	On extreme compositions
Apatite Early Stage	Apatite	8/420	LAM1, LAM2, FOJ, RUD1, RUD2, VRE, MIL, EQU	3	Varimax axes
Apatite Middle Stage	Apatite	9/284	LAM1, ENK1 to ENK5, BUK, SPH, EQU	3	On extreme compositions
Apatite Late Stage	Apatite	4/163	LAM1, SOK, GRU, EQU	3	On extreme compositions

Table 4. Chemical composition of generated end-members in run Whole-rock All. Major element are given in wt%, trace elements in ppm.

	EM1	EM2	EM3
SiO_2	79.82	53.47	52.14
TiO_2	0.00	1.57	1.85
Al_2O_3	11.51	18.01	17.79
Fe_2O_3	0.00	9.02	11.27
MnO	0.00	0.12	0.21
MgO	0.00	4.05	4.22
CaO	0.00	6.02	6.33
Na_2O	2.80	3.95	5.70
K_2O	5.83	3.00	0.00
P_2O_5	0.00	0.49	0.40
Rb	297	92	293
Ba	17	1431	60
Th	32	11	2
Nb	8	22	42
Sr	0	624	137
Zr	42	431	306
Y	31	44	102
Ni	0	51	13
La	11	95	0
Ce	28	177	0
Nd	12	73	6
Sm	3	12	4
Eu	0	2	0
Gd	4	9	5
Dy	5	7	6
Er	3	3	4
Yb	4	2	4
Lu	1	0	1

Table 5. Coefficients of Determination (KMCD) for two, three and four end-members in run Whole-rock All.

Number of end-members	2	3	4
SiO_2	0.93	0.92	0.92
TiO_2	0.87	0.87	0.89
Al_2O_3	0.69	0.84	0.93
Fe_2O_3	0.92	0.89	0.89
MnO	0.63	0.72	0.72
MgO	0.79	0.85	0.89
CaO	0.92	0.95	0.97
Na_2O	0.26	0.79	0.81
K_2O	0.47	0.71	0.77
P_2O_5	0.66	0.73	0.75
Rb	0.23	0.60	0.66
Ba	0.29	0.78	0.93
Th	0.56	0.64	0.71
Nb	0.18	0.36	0.37
Sr	0.40	0.67	0.69
Zr	0.22	0.74	0.82
Y	0.02	0.60	0.60
Ni	0.30	0.53	0.67
La	0.11	0.87	0.87
Ce	0.08	0.88	0.90
Nd	0.14	0.88	0.91
Sm	0.08	0.83	0.88
Eu	0.18	0.50	0.52
Gd	0.02	0.75	0.84
Dy	-0.02	0.66	0.73
Er	0.00	0.63	0.70
Yb	0.04	0.63	0.69
Lu	0.03	0.59	0.64

Table 6. Chemical composition of generated apatite end-members.

Run	Apatite Early Stage			Apatite Middle Stage			Apatite Late Stage		
End-member	**EM1**	**EM2**	**EM3**	**EM1**	**EM2**	**EM3**	**EM1**	**EM2**	**EM3**
P2O5	41.58	34.89	39.33	40.81	34.15	39.51	41.04	37.72	39.47
SiO2	0.00	3.63	0.30	0.02	3.77	0.80	0.31	1.68	0.92
ThO2	0	0.09	0.01	0	0.19	0.01	0	0.04	0.01
UO2	0	0.08	0.05	0.01	0.04	0.04	0.01	0.01	0.04
Y2O3	0	2.56	0	0.14	3.42	0	0.02	1.08	0.00
La2O3	0	0.56	0.23	0	0.61	0.08	0	0.48	0.04
Ce2O3	0	1.92	0.38	0.01	1.62	0.12	0	1.31	0.09
Pr2O3	0	0.34	0.03	0.01	0.30	0.01	0	0.20	0.02
Nd2O3	0	1.52	0.10	0.02	1.50	0.03	0.0007	0.90	0.05
Sm2O3	0	0.43	0.06	0	0.55	0.02	0	0.26	0.02
Yb2O3	0	0.16	0	0.0011	0.32	0	0.01	0.06	0.00
CaO	53.17	49.75	55.48	54.33	49.79	54.54	54.19	52.34	54.46
MnO	0.15	0.11	0	0.19	0	0.04	0.12	0.08	0.08
FeO	0.41	0.22	0	0.30	0	0.34	0.35	0.10	0.45
SrO	0	0	0.54	0.00	0	0.25	0.00	0	0.20
Na2O	0.10	0.03	0.15	0.15	0.06	0.34	0.08	0.08	0.29
SO3	0	0	0.56	0	0	0.57	0	0	0.45
F	4.60	3.70	0.27	3.99	3.70	1.15	3.87	3.65	1.72
Cl	0	0	1.22	0	0	1.26	0	0	1.00
H2O	0	0	1.30	0	0	0.89	0	0	0.69

Table 7. Coefficients of Determination (KMCD) for two, three and four end-members in runs Apatite Early, Middle and Late Stage.

	Apatite Early Stage			Apatite Middle Stage			Apatite Late Stage		
Number of end-members	2	3	4	2	3	4	2	3	4
P_2O_5	0.56	0.65	0.66	0.17	0.48	0.48	0.06	0.62	0.65
SiO_2	0.42	0.53	0.56	0.08	0.26	0.27	0.04	0.41	0.44
ThO_2	0.43	0.45	0.45	0.05	0.12	0.12	0.07	0.27	0.30
UO_2	0.09	0.12	0.84	-0.00	0.05	0.05	0.03	0.11	0.92
Y_2O_3	0.67	0.79	0.79	0.50	0.74	0.79	0.25	0.67	0.77
La_2O_3	0.45	0.58	0.59	0.18	0.54	0.55	0.26	0.61	0.64
Ce_2O_3	0.77	0.85	0.85	0.38	0.64	0.65	0.38	0.74	0.77
Pr_2O_3	0.45	0.47	0.62	0.15	0.32	0.74	0.22	0.39	0.39
Nd_2O_3	0.82	0.85	0.85	0.48	0.71	0.71	0.47	0.81	0.82
Sm_2O_3	0.54	0.56	0.56	0.32	0.51	0.79	0.27	0.61	0.61
Yb_2O_3	0.30	0.40	0.41	0.30	0.48	0.55	0.12	0.21	0.32
CaO	0.45	0.68	0.69	0.15	0.41	0.42	0.17	0.60	0.60
MnO	0.00	0.47	0.51	0.00	0.63	0.64	0.00	0.68	0.68
FeO	-0.00	0.32	0.36	0.00	0.06	0.12	0.04	0.64	0.65
SrO	0.01	0.18	0.18	0.54	0.92	0.93	0.73	0.92	0.92
Na_2O	0.03	0.69	0.71	0.14	0.36	0.58	0.35	0.58	0.59
SO_3	0.08	0.80	0.80	0.51	0.85	0.86	0.66	0.91	0.91
F	0.03	0.95	0.95	0.49	0.96	0.96	0.66	0.97	0.98
Cl	0.05	0.85	0.85	0.53	0.95	0.95	0.68	0.96	0.96
H_2O	0.04	0.89	0.89	0.51	0.93	0.93	0.68	0.96	0.96

Highlights:

- We use apatite composition compared to whole-rock chemistry to trace magma mixing
- We use Polytopic Vector Analysis for both whole-rock and apatite chemistry
- PVA of whole-rock chemistry shows a combination of all differentiation processes
- Apatite composition is too complex to be decomposed into end-members by PVA
- PVA requires basic knowledge on magma evolution of the studied igneous system